Timing of syn-orogenic extension in the Western Alps revealed by calcite U-Pb and hematite (U-Th)/He dating

Antonin Bilau, Yann Rolland, Stéphane Schwartz, Cécile Gautheron, Thierry Dumont, Dorian Bienveignant, Benjamin Brigaud, Nicolas Godeau, Abel Guihou, Pierre Deschamps, et al.

Geoscience Frontiers 16 (2025) 101969

Contents lists available at ScienceDirect

Geoscience Frontiers

journal homepage: www.elsevier.com/locate/gsf

Research Paper

Timing of syn-orogenic extension in the Western Alps revealed by calcite U-Pb and hematite (U-Th)/He dating

Antonin Bilau [a,b,*], Yann Rolland [a,b], Stéphane Schwartz [b], Cécile Gautheron [b,c], Thierry Dumont [b], Dorian Bienveignant [b], Benjamin Brigaud [c], Nicolas Godeau [d], Abel Guihou [d], Pierre Deschamps [d], Xavier Mangenot [d,e], Marianna Corre [b], Rosella Pinna-Jamme [c], Nathaniel Findling [b]

[a] EDYTEM, Université Savoie Mont Blanc, CNRS, UMR 5204, Le Bourget du Lac, France
[b] ISTerre, Université Grenoble Alpes, USMB, CNRS, IRD, UGE, Grenoble, France
[c] GEOPS, CNRS, Université Paris-Saclay, 91405 Orsay, France
[d] Aix-Marseille Université, CNRS, IRD, INRAE, CEREGE Collège de France, Aix-en-Provence, France
[e] Caltech, Geological and Planetary Sciences, Pasadena, CA, USA

ARTICLE INFO

Article history:
Received 13 March 2024
Revised 28 September 2024
Accepted 14 November 2024
Available online 27 November 2024
Handling Editor: S. Glorie

Keywords:
Western Alps
Briançonnais zone
Hematite (U-Th)/He
U-Pb calcite
Clumped isotopes
Syn-orogenic extension

ABSTRACT

Understanding fault activity over time provides valuable insights for reconstructing the tectonic history of an orogen, assessing seismological risks and understanding mineralization processes. In the Western Alps, one of the main controversies in existing tectonic models is the understanding of *syn*-orogenic extension. Seismological evidence shows widespread extensional deformation related to the reactivation of major lithospheric structures, such as the Penninic Frontal Thrust (PFT). However, the onset age and origin of extension are still debated due to the lack of suitable geochronological data. Fault hematite and calcite geochronology as well as clumped isotope data can be used to relate fluid regimes to fault activity. The analysis of calcite brecciae from extensional faults above the PFT shows that two distinct fluid regimes were present. The first regime, occurring before 2 Ma is associated with upwelling of deep fluids and is recorded by fault calcite at a temperature > 110°C. The second fluid regime is characterized by a meteoric signature and temperatures around 36 °C, representing crystallization since 2 Ma. This study presents a new model for the Miocene tectonic history of the Western Alps that combines (U-Th)/He and U-Pb geochronology on fault hematite (13.3 ± 0.8 to < 0.8 Ma) and calcite (5.3 ± 0.6 Ma). Results demonstrate a progression of extensional fault activity from east to west, from the Middle Miocene (ca. 13 Ma) to the Quaternary. The onset of extension in the inner part of the belt coincides with the development of the fold and thrust belt in the western Alpine foreland. Our new model proposes that extension occurs in the hanging wall of a large top-to-the-west thrust, known as the Alpine Frontal Thrust. This thrust, located to the west of the External Crystalline Massifs gives rise to their uplifting and extension at the rear.

1. Introduction

The tectonic evolution of fault networks can be constrained by using geochronological methods on minerals formed during fault activity. Among these, calcite and hematite are classically observed on surfaces of tectonic structures (fault veins, fibers, striae etc.) and can be dated by U-Pb on calcite (Roberts et al., 2017) or by (U-Th)/He dating on hematite (e.g., Wernicke and Lippolt, 1994; Evenson et al., 2014; McDermott et al., 2017, 2021; Ault, 2020). These methods can give crystallization ages related to the development of brittle deformation during fault activity (e.g., Roberts and Walker, 2016; Beaudoin et al., 2018; Parizot et al., 2021; Roberts and Holdsworth, 2022; Bilau et al., 2023a, b; Lacombe and Beaudoin, 2024). Additionally, $\delta^{18}O$, $\delta^{13}C$ isotopes and Δ_{47} clumped isotopes on calcite provide information about the composition and temperature of the precipitating fluids (e.g., Bonifacie et al., 2017; Pagel et al., 2018).

In this study, we combine geochronological methods with stable isotope analyses to document the relationship between fluid and fault history. This study focusses on the High-Durance Fault

* Corresponding author.
E-mail address: antonin.bilau@kit.edu (A. Bilau), antonin.bilau@kit.edu (A.

https://doi.org/10.1016/j.gsf.2024.101969

System, a significant transtensional fault complex in the Briançonnais zone of the Western Alps (Fig. 1), which is currently active (Sue and Tricart, 2003; Sue et al., 2007). The extensional faults of this complex cross-cut and partly reactivate some of the previous crustal-scale Alpine structures like the Penninic Frontal Thrust (PFT). Extensional activity is confined to the core of the Alpine belt, which is still undergoing uplift, raising questions about the timing of the extensional deformation in a collisional context (e.g., Tricart et al., 2006). Some authors have proposed that the presence of extension is explained by an extensional collapse after a phase of collisional thickening (e.g., Selverstone, 2005). However, in the case of the Western Alps, the current strain field is dominated by a strike-slip context with a strong partitioning of deformation highlighted by compression on their forelands (Malusà et al., 2017, 2021; Mathey et al., 2021; Schwartz et al., 2024). Extension appears to be *syn*-orogenic and contemporaneous with strike-slip and compression tectonics in the Alpine foreland. However, the onset of extension remains temporally unconstrained, which leads to controversial interpretations (Larroque et al., 2009; Bauve et al., 2014). Further, driving forces for *syn*-orogenic extension are still a matter of debate (Sternai et al., 2019). The driver of the extensional component of the strain field could result from various processes such as a decrease in compressive stress (Selverstone, 2005), slab breakoff (von Blanckenburg and Davies, 1995), crustal overcompensation or isostatic rebound due to erosion or glacial melting (e.g., Champagnac et al., 2007; Sternai et al., 2019), or mantle indentation of the orogenic wedge and Adria counterclockwise rotation (Schwartz et al., 2024).

In the Briançonnais zone, the extensional domain is localized to the east of the Pelvoux Massif (Tricart et al., 2001; Lardeaux et al., 2006). This extension could result from a local accommodation at the back of a crustal-scale thrust related to the propagation of the belt towards its foreland in a thick-skinned mode (Bilau et al., 2023a). It would therefore be the result of a deep tectonic process rather than a surface re-adjustment related to erosional processes (e.g., Vernant et al., 2013). However, it is still difficult to discuss the potential causality of thick-skinned tectonics trigger and the development of *syn*-orogenic extension in the Western Alps as the age of extension initiation is still unconstrained. The timing of brittle deformation stages is primarily constrained by indirect dating techniques, such as fission track thermochronology (e.g., Tricart et al., 2007).

The objective of this study is to provide definitive temporal constraints on the initiation of extensional processes that have occurred during the tectonic reactivation of the PFT. Additionally, the aim is to examine the chronological relationship between these processes and the development of the frontal Alpine fold and thrust belt and the exhumation of the External Crystalline Massifs (ECM). In this paper, we provide geochronological constraints based on U-Pb calcite and (U-Th)/He hematite data within the Briançonnais zone, which allow to discuss the onset and propagation of extension within the High-Durance Fault System. In addition, clumped isotope analysis performed on calcite from the same dated sites give insights into the related regional fluid circulation context (e.g., Smeraglia et al., 2022; Bilau et al., 2023a). The new data are further discussed in the structural context of the Western Alps and its European foreland.

2. Geological setting

The western Alpine belt resulted from the convergence and collision of the European and Adriatic plates (e.g., Tricart, 1984) since Cretaceous time. The internal zones (Fig. 1) are characterized by High-Pressure – Low-Temperature (HP-LT) metamorphic conditions related to the subduction of the paleo-distal European margin of the Briançonnais zone and oceanic-derived units of the Piedmont zone (Schwartz et al., 2009; Dumont et al., 2022). The Briançonnais zone is composed of Mesozoic and Paleozoic

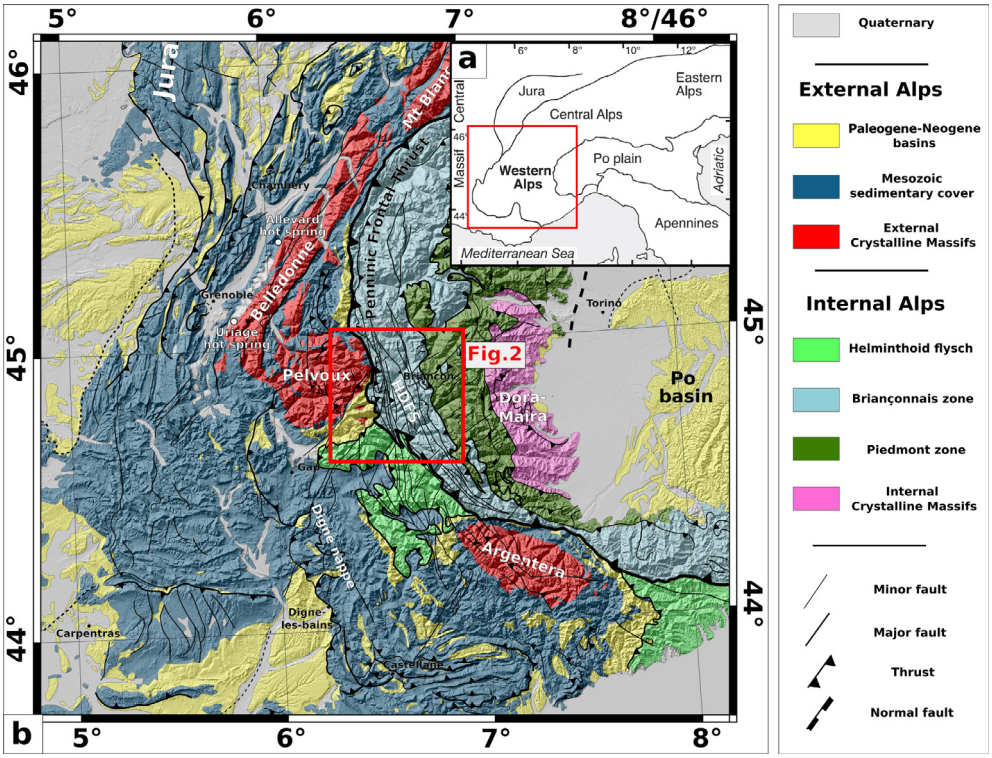

Fig. 1. (a) Location of the Western European Alps. (b) Geological map coupled to a DEM of the Western Alps of the study area (red rectangle, for closer map, see Fig. 2). The main faults structuring the foreland and the inner part of the belt are indicated. The Briançonnais zone is crosscut by the High-Durance Fault System (HDFS), which develops along the Penninic Frontal Thrust. (For interpretation of the references to color in this figure legend, the reader is referred to the web version of this article.)

sedimentary units derived from the thinned European continental margin (Manatschal, 2004). This zone corresponds to a stack of exhumed and folded metamorphic nappes with opposite vergence on either side (Dumont et al., 2022).

The external zones comprise the sub-greenschist facies (e.g. Frey and Ferreiro Mählmann, 1999) European Mesozoic sedimentary cover and its Paleozoic basement corresponding to the ECMs. Collisional dynamics led to a major lithospheric-scale tectonic structure, the PFT (e.g., Tardy et al., 1990), which was active in Late Eocene to Oligocene times (Dumont et al., 2012, 2022; Bellahsen et al., 2014). The PFT accommodated the westward thrusting of the internal over the external zones at 34–31 Ma (Schmid and Kissling, 2000; Ceriani et al., 2001; Ceriani and Schmid, 2004; Lardeaux et al., 2006; Simon-Labric et al., 2009). Ambient noise Vs tomography (Nouibat et al., 2022; Schwartz et al., 2024) highlights the deep structure of the chain. To the East of the PFT, in the internal zones representing a subduction wedge, the crustal geometry shows the presence of a European continental slab that was locally subducted to more than 80 km beneath the Adria plate in the SW part of the Alpine arc. The Moho morphology is characterized by two mantle indenters located above the subducted European plate at different depths, which appear to control the locus of active deformation. The rigid nature of the Adriatic mantle explains the localization of brittle deformation that is transferred towards the upper crust. The strain field partitioning results in a combination of strike-slip with either shortening or extension controlled by the displacements imposed by the current NW/SE convergence associated with the anticlockwise rotation of Adria (see Schwartz et al., 2024 for details). In this context, the High Durance Fault System corresponds to a cluster of normal faults reactivating the PFT and partly cross-cutting it at depth (Sue et al., 2007). In detail, this fault cluster is bounded by two main branches on both sides of the Briançonnais zone. To the east, the Clarée Fault Zone (CFZ) and to the west, along the PFT, the High Durance fault Zone (HDZ). Near Tournoux (Fig. 2), the HDZ branch on the PFT, while more to the south, at Plan de Phazy, the HDZ crosscuts the PFT (Sue and Tricart, 2003; Thouvenot and Fréchet, 2006; Sue et al., 2007). Present-day seismicity is distributed along lineaments whithin the High Durance Fault System and mostly clusters at shallow depths of 3 to 8 km, where the faults are structurally connected to the PFT (Sue and Tricart, 2003; Thouvenot and Fréchet, 2006; Sue et al., 2007). Focal mechanisms show a combination of strike-slip and extensional components consistent with a regional transtensional tectonic regime (Sue et al., 2007). Ongoing deformation is highlighted by observed GPS motions (Walpersdorf et al., 2018; Mathey et al., 2021, 2022). The analysis of GPS velocity profiles highlights zones of extension in the center of the belt localized in the Briançonnais zone, and shortening in the foreland (Walpersdorf et al., 2018). In the ECMs, the main observed component corresponds to vertical motions of 0.5 to 3.0 mm per year.

The onset of compressive tectonic activity along the PFT is constrained to 34 Ma based on *syn*-kinematic Ar-Ar ages on phengite, U-Pb ages on allanite and on reset zircon (U-Th)/He ages in the PFT fault zone (Simon-Labric et al., 2009; Cenki-Tok et al., 2014; Bellanger et al., 2015; Maino et al., 2015). Apatite fission track (AFT) ages from the Briançonnais zone range from 31 Ma to 22 Ma (Fig. 2; Tricart et al., 2001, 2007) and suggest that the exhumation of the Briançonnais zone is related to reverse faulting along the PFT. The younger AFT ages in the Briançonnais zone between 10 and 15 Ma are related to the circulation of hot fluids

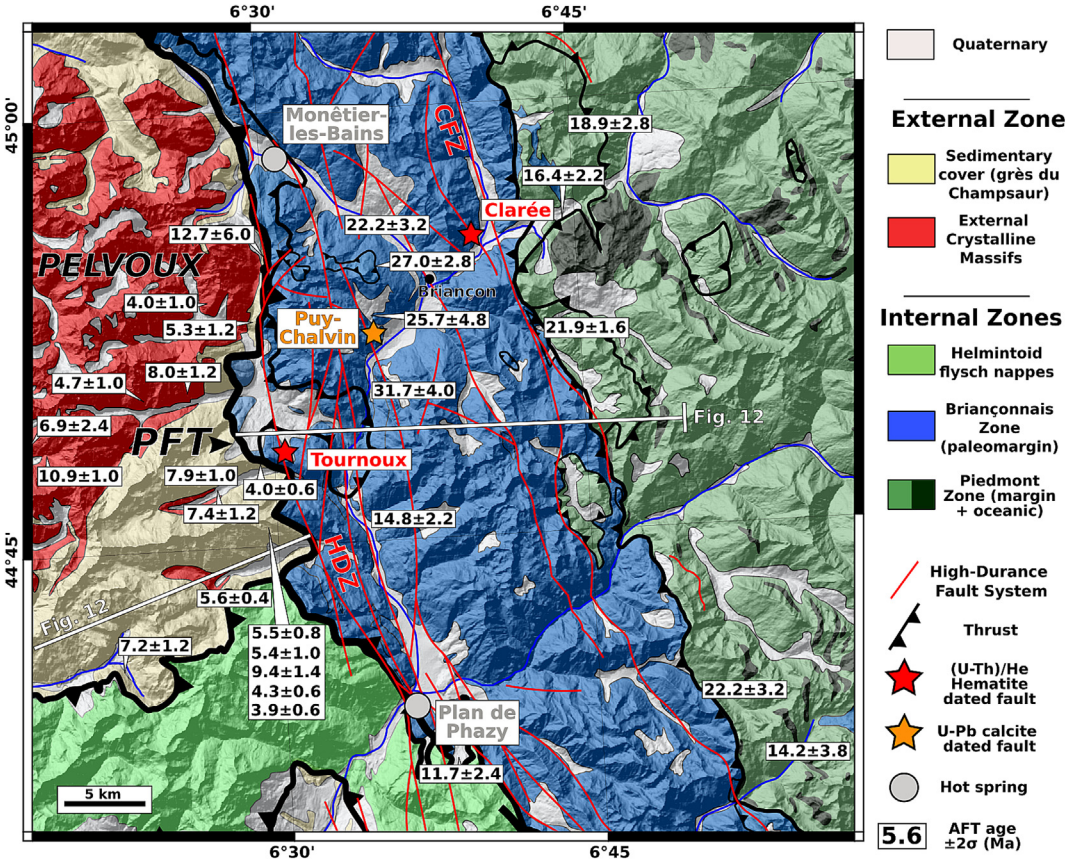

Fig. 2. Geological map coupled to a DEM of the study area with location of the High-Durance Fault System and the Penninic Frontal Thrust (PFT), modified after Tricart (2004), with its eastern (Clarée Fault Zone, CFZ) and western branch (High-Durance Zone, HDZ). The orange stars indicate calcite U-Pb dating sites and red stars indicate hematite (U-Th)/He dating sites. The main regional hot springs are indicated by grey circles. Numbers in white retangles correspond to AFT ages (in Ma) from Tricart et al. (2007) and Seward et al. (1999). (For interpretation of the references to color in this figure legend, the reader is referred to the web version of this article.)

circulating along the HDZ, with temperatures exceeding 80 °C (Fig. 2, Tricart et al., 2007).

The onset of extension in the Briançonnais zone is still poorly constrained. Several authors proposed that the transition from compression to extension took place in the age range of ca. 15 Ma to 5 Ma, on the basis of the AFT ages obtained in the PFT footwall (Fig. 2) related to the ECMs exhumation (Tricart et al., 2001, 2006, 2007; Schwartz et al., 2007). Calcite U-Pb dating on the HDZ highlights several brittle events between 3.6 ± 0.4 Ma and 2.3 ± 0.2 Ma, and provides a minimum age for the onset of extension within the High-Durance Fault System (Bilau et al., 2021).

3. Methods

3.1. Sampled sites along the High-Durance Fault System

Three sites were sampled from east to west in the Briançonnais zone along the High-Durance Fault System in order to collect hematite and calcite formed during fault activity: the Clarée, the Puy-Chalvin and the Tournoux sites. Those samples complement the U-Pb and Δ_{47} data from the same area by Bilau et al. (2021). Sample names, mineralogical characteristics and locations are reported in Table 1. Structural measurements are displayed in the Supplementary Data 1. Additional mineralogical and major-trace element analyses of the samples are reported in the Supplementary Data 2 and 3.

3.1.1. Clarée site

At the Clarée site, the CFZ (Fig. 3a) can be traced at the surface across Bathonian-Callovian bioclastic limestone locally karstified and filled by iron-rich red micrite. The sample fault zone is highlighted by a thick reddish zone of > 100 m length (Fig. 3a). Bedding is tilted by ~ 40° to the west (Fig. 3b) and the paleokarst formation occurred after folding. The fault system runs NNW-SSE with a dip of 80° – 50° to the southwest. The fault exhibits strike-slip to normal slip and affects local karst fillings that are located in the core of a syncline. Motions along the CFZ fault show overprinting relationships with alternating pure strike-slip and extensional stress regimes (Fig. 3b). The fault zone runs along the valley for several kilometers and has a width of several tens of meters, with numerous striated planes and tectonic breccias. It cuts through paleokarst fillings and has remobilized some of the iron-rich material. Hematite and calcite mineralization has been observed and both sampled in two habitus (veins and striated planes). The vertical veins branch into the fault planes, and are thus kinematically coherent to the same extensional fault motions. In the veins, calcite systematically crystallizes before hematite. Three hematite samples have been selected for hematite (U-Th)/He (H/He) analysis. The calcite samples taken from fault planes and veins proved unsuitable for dating.

3.1.2. Puy-Chalvin site

The samples were collected along an extensional fault affecting Lower Triassic quartzites in the central part of the Briançonnais zone, located on the eastern edge of the HDZ (Fig. 2, Puy-Chalvin site). Fault planes are vertical to steeply dipping to the SE. The fault strike is oriented SW-NE, with striations showing normal and partly strike-slip motions (down dip to 45° towards NE, Fig. 4). These fault geometry and kinematics correspond to the commonly observed features of extensional faults within the High-Durance Fault System (e.g., Mathey et al., 2020). In this site, the present study has not yielded any results that would allow for the dating of hematite. However, the dating of calcite has been successful.

3.1.3. Tournoux site

On the western edge of the Briançonnais zone, along the HDZ, in the hanging wall of the PFT (internal Alps), the Tournoux site (Figs. 2, 5a) was investigated as a complement to previous work by Bilau et al. (2021) from the same location (in outcrop 1, Fig. 5). Calcite-filling fault samples were selected for Δ_{47} analysis in relation to the previous samples from Bilau et al. (2021) and the obtained U-Pb ages of 3.6 ± 0.4 Ma and 2.3 ± 0.2 Ma (Table 1). To the east of Tournoux site (outcrop 2), close to the Col de la Pousterle and 400 m away from Tournoux outcrop 1, samples were retrieved from an outcrop of a normal fault, which roots down into the PFT (Fig. 5a). The fault offset is about 300 m and juxtaposes brecciated whitish Triassic quartzites next to Upper Cretaceous calcschists (Sue and Tricart, 1999, Fig. 5b). The fault zone contains a breccia with clasts of stretched Triassic dolomitic limestones cemented by a first generation of calcite (Fig. 5c). This breccia is cut by hematite veins several millimetres wide. The hematite was striated by later fault plane activity and underwent recrystallization. Twenty samples of striated fault planes (centimetre-long) were collected, composed of layers of hematite interlayered with phyllosilicates (Fig. 5d). A first relative chronology at the scale of the outcrop can be established (Fig. 5c) with (1) calcite precipitation, (2) crosscut by hematite veins, and (3) striated hematite on the fault plane. Similar to the Clarée site, hematite is found to be the most recent precipitation product.

3.2. Scanning electron microscope imaging

Hematite samples of cm-scale were photographed under a binocular microscope and mounted for scanning electron microscope (SEM) analysis. For most samples, observations perpendicular to fault striation were made using the SEM Vega 3 Tescan of ISTerre (University Grenoble Alpes, France). BSE and EDS where used to identify the most Fe-rich zones and then a detailed image was made to characterize the crystallite sizes. Acquisition parameters were optimized on each picture in order to reach a ~ 20 nm resolution. Crystallite sizes of hematite were measured

Table 1
Sample coordinates and information.

Briançonnais zone	Name	Latitude (°N)	Longitude (°E)	Elevation (m)	Sample type	Analyses done	Reference
East	Clarée	44°55′27.52″	6°39′44.34″	1815	hematite fault and vein	mineralogy, geochemistry, (U-Th)/He	this study
Central	Puy-Chalvin	44°52′36.23″	6°34′44.17″	1546	calcite fault	calcite U-Pb,	this study
West	Tournoux outcrop 1	44°48′29.75″	6°30′31.38″	1910	calcite fault	Δ_{47}	this study
						calcite U-Pb	Bilau et al. (2021)
	Tournoux outcrop 2	44°47′55.70″	6°30′53.30″	1641	hematite fault and vein	mineralogy, geochemistry, (U-Th)/He	this study
					calcite fault	Δ_{47}	this study

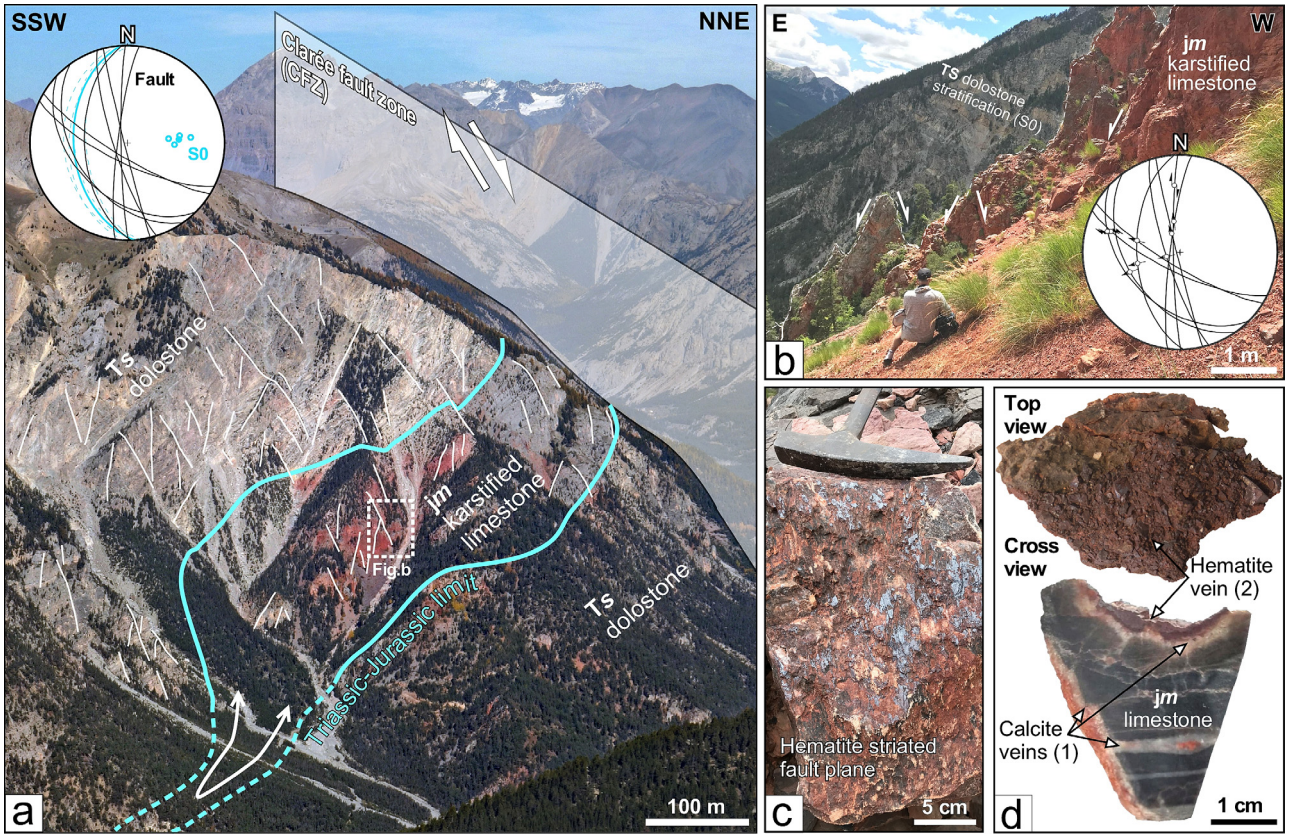

Fig. 3. (a) General view to the western side of the Clarée Valley. Blue lines correspond to the main bedding highlighting a syncline within the Upper Trias (Ts) and Middle Jurassic (jm) rocks. White lines correspond to normal faults. These faults (in black) and the average bedding (in blue) are displayed in the Schmidt stereogram (lower hemisphere). (b) Outcrop whithin the karstified limestones crosscut by normal faults related to the CFZ. The faults and the corresponding striae are shown in the Schmidt stereogram. Fault plane data are available in the Supplemetary Data 1. (c) Close-up of a sampled hematite striated fault plane. (d) Views of calcite and hematite veins showing that hematite crystallized after calcite. (For interpretation of the references to color in this figure legend, the reader is referred to the web version of this article.)

on more than twenty images and mean values are reported in Supplementary Data 4.

3.3. Hematite (U-Th)/He geochronology

H/He dating was undertaken at the GEOPS laboratory (University Paris Saclay, France). Centimetre-scale hematite vein and striated hematite plane samples (Clarée: 2 samples, Tournoux: 17 samples) were selected for (U-Th)/He dating based on color and luster as a proxy for the highest amount of hematite. These samples were fragmented in ~ 500 μm size aliquots in order to compensate the He ejection distance (Ketcham et al., 2011). Six aliquots from Clarée and 53 for Tournoux site were analysed. Whenever possible, several aliquots from the sample sampling site were retrieved and a distance from the fault striated plane was estimated. Hematite grains were cleaned with ethanol in an ultrasonic bath and by additional analyses on the same sample it was checked that no He loss was caused by the treatment. Aliquots were weighed using a Mettler Toledo balance and their sizes were measured under a binocular microscope. Aliquots of 200–500 μm with weights ranging from 150 to 1020 μg were selected and He was extracted at a temperature < 900 °C for 30 min to avoid volatilization of U during degassing (Danišík et al., 2013; Hofmann et al., 2020). The He, U, Th and Sm contents were obtained using protocols described in Allard et al. (2018) and Gautheron et al. (2021), and concentration obtained using the aliquote measured weight. Error on He is currently < 2% but could get up to 10% depending on He content. U, Th and Sm contents are < 2%, and error on uncorrected H/He age is ranging from 6% to 10%. Accuracy of the procedure is monitored by the analysis of Durango apatite and an internal goethite standard samples. A 5% He loss correction was applied to the (U-Th)/He age with an 10% error added to the analytical error to include He loss associated with crystallite size heterogeneity and phase mixing within the samples (Heller et al., 2022). All data are listed in Supplementary Data 4.

3.4. Calcite U-Pb geochronology

In-situ U-Pb calcite analyses were carried out at the CEREGE (Centre Européen de Recherche et d'Enseignement des Géosciences de l'Environnement, Aix-en-Provence, France) using a Thermo Fisher Scientific, Element XR, and a 193 nm laser wavelength, 0.8 to 1.4 J·cm^{-2} fluence and 10 Hz repetition rate. The carrier gas was composed of 100% He 5.0 – 0.9 L·min^{-1}, Ar make-up gas ~ 1 L·min^{-1} combined using a Y-piece ~ 50 cm before the connection to the injector. The laser spot size was 150 μm and firing for 20 s lead to a ~ 30 μm downhole (see Bilau et al., 2023a for futher details). A NIST-614 glass standard was used as primary reference material for drift and Pb isotopes; WC-1 carbonate served as a reference material for matrix matching of $^{206}Pb/^{238}U$ and B6 as secondary material (Roberts et al., 2017; Pagel et al., 2018; Brigaud et al., 2021). For data processing, raw intensities and baseline correction were made with the Iolite 3 baseline DRS (Paton et al., 2011). Instrumental drift based on NIST-614 analyses (Woodhead and Hergt, 2001), Pb isotopes composition and $^{206}Pb/^{238}U$ are calculated using an in-house Python code. Tera-Wasserburg plots, calculation of intercept ages and initial Pb compositions were made

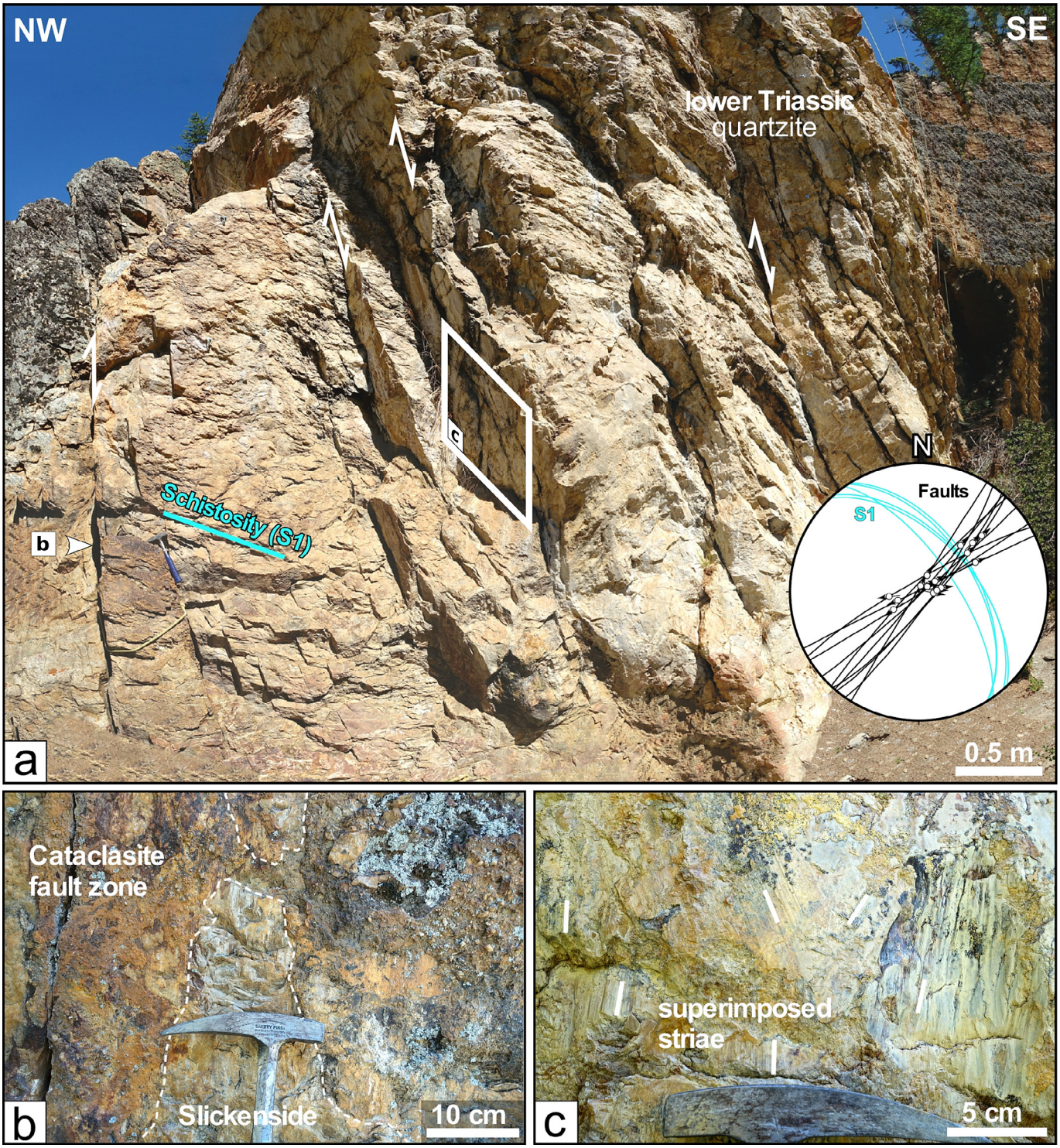

Fig. 4. Photographs and structural data of the calcite fault breccia dated by U-Pb on calcite at the Puy-Chalvin site. (a) Photograph of normal faults cutting through the Triassic quartzites. The schistosity orientation (S1) is shown by the cyan line and the sense of shear are indicated by the white arrows. Structural data (schistosity S1 in blue and faults in black) are plotted on a Schmidt stereogram (lower hemisphere). (b) Example of the sampled fault zone showing a cataclasite with calcite cement (corresponding to the dated sample in Fig. 8) and slickensides. (c) Striated fault plane mineralized by calcite and showing tectoglyphs indicative of superimposed normal and partly transcurrent slip. (For interpretation of the references to color in this figure legend, the reader is referred to the web version of this article.)

using IsoplotR (model-1) (Vermeesch, 2018). Ages are quoted with 2σ absolute error with propagation of WC-1 2.51% age error by quadratic addition (Roberts et al., 2017). Excess variance within the reference material was considered and systematic uncertainties included the age uncertainty of reference material. Data are reported in Supplementary Data 5.

3.5. Stable isotope analysis

Two brecciated calcite samples from the Tournoux outcrop 1 and one sample from outcrop 2 were selected for clumped isotopes (Δ_{47}) analyses (Table 2). Thirty milligrams of pure calcite was retrieved using a Dremel on each of the three samples in order to

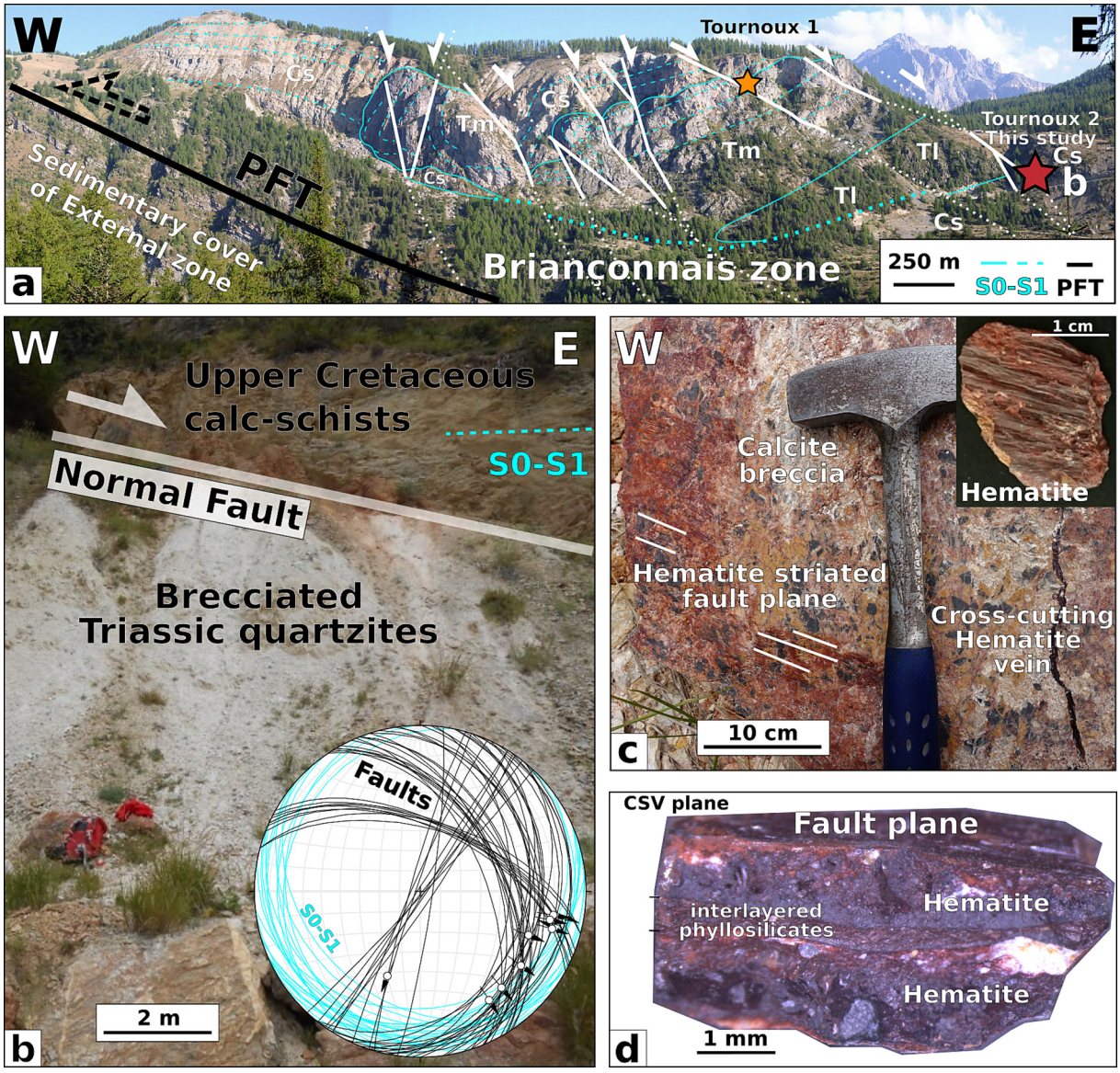

Fig. 5. (a) General view of the Tournoux 1 and 2 sampling sites in the hanging-wall of the Penninic Frontal Thrust. The orange star to the left refers to the older faults dated on breccia calcite (Tournoux outcrop 1, 3.6 ± 0.4 Ma to 2.3 ± 0.2 Ma, errors = 2σ), while the red star to the right refers to Tournoux outcrop 2 with the younger fault (<2 Ma) passing across the Pousterle Pass. Cs: Late Cretaceous calcschists; Tm: Middle Triassic dolomitic limestones; Tl: Lower Triassic sandstones. White lines correspond to High-Durance Zone normal faults. (b) Outcrop view of the Tournoux outcrop 2, the normal fault is highlighted by the tectonic contact of Upper Cretaceous calc-schists on top of Triassic quartzites. The orientation of the fault planes and related striae are plotted in the Schmidt stereogram (lower hemisphere). Measured faults show conjugate orientations with a consistent normal (and minor strike-slip) motion deduced from striae and slickenside relationships. The orientation of the Upper Cretaceous schistosity is shown in blue, and is close to horizontal (S1 parallel to S0). (c) Fault breccia showing relative cross-cutting relationships of a first generation of calcite cementing darker clasts of the host rock, intersected by a hematite vein and then striated by the activity of the fault plane coated with hematite. (d) Cross-section view (CSV) of the hematite-bearing fault plane sample showing multiple bands of hematite. (For interpretation of the references to color in this figure legend, the reader is referred to the web version of this article.)

extract and analyse CO_2 at CalTech (USA). Each Δ_{47} analysis was replicated. Eight milligrams of calcite powder were placed in a silver capsule and dissolved under static vacuum in a bath of phosphoric acid for 20 min at 90°C. The produced CO_2 was collected via a U-shaped trap at a temperature of −196 °C. The CO_2 was then transported with a helium flux through a Porapak Q 120/80 mesh separation column at −20°C. After purification, the 44 − 49 masses of CO_2 were measured with a Thermo Scientific MAT 253 Mass Spectrometer. The $\delta^{13}C$ and $\delta^{18}O$ isotope ratios were also measured via gas standards analysis and calibrated against PDB standard. The raw data were corrected for fractionation by acid dissolution at 90 °C with a fractionation factor of 1.00811 (Swart et al., 1991) as well as instrumental drift, and all results are expressed in the inter-laboratory reference frame, $\Delta_{47\text{-CDES25}}$ (Dennis et al., 2011; Bonifacie et al., 2017). During the analysis sessions, 8 samples of Carrara marble showed $\Delta_{47\text{-CDES25}}$ results of 0.394‰ ± 0.012‰ (1σ), and 10 samples of carbonate TV04 showed $\Delta_{47\text{-CDES25}}$ results of 0.653‰ ± 0.017‰ (1σ). These results correspond to accepted values for these standards: $\Delta_{47\text{-CDES25}}$ = 0.655‰ for TV04 and $\Delta_{47\text{-CDES25}}$ = 0.405‰ for Carrara (Mangenot et al., 2024). The error related to the standards was used (± 0.014‰, 1σ) for samples without 3 replicates. Finally, the corrected Δ_{47} measurements were converted to temperature using the equation of Bonifacie et al. (2017) and results are reported in Table 3. Assuming that this temperature is a crystallization temperature and that the system remained closed, the $\delta^{18}O$ signature of the calcite mineralizing fluid is calculated using the Kim and O'Neil (1997) equation (Table 3).

Table 2
Clumped isotope results on calcite from Tournoux site tectonic breccia and calculated temperatures. $\Delta_{47\text{-CDES90}}$ correspond to Carbon Dioxide Equilibrium Scale with acid digestion at 90°C, SMOW = Standard Mean Ocean Water, VPDB = Vienna Pee Dee Belemnite. U-Pb calcite ages for FP18-2B and FP18-3A are from Bilau et al. (2021).

Location	Name	U-Pb age	$\delta^{18}O_{calcite}$ (SMOW)	$\delta^{13}C_{calcite}$ (VPDB)	$\Delta_{47\ CDES90}$	$1\sigma\ \Delta_{47}$	$\Delta_{47\ min}$	$\Delta_{47\ max}$	T(°C)	T_{min}(°C)	T_{max}(°C)
Tournoux outcrop 1	FP18-2B	3.4 ± 1.4 Ma	8.70	−0.09	0.41						
			8.32	−0.10	0.38						
			8.51	**−0.10**	**0.39**	**0.014**	**0.379**	**0.407**	**125**	**115**	**135**
	FP18-3A	2.3 ± 0.2 Ma	9.10	−1.46	0.39						
			9.11	−1.44	0.38						
			9.11	**−1.45**	**0.38**	**0.007**	**0.376**	**0.389**	**133**	**128**	**138**
Tournoux outcrop 2	calcite cement	no data	13.75	−1.18	0.57						
			13.77	−1.20	0.56						
			13.86	−1.26	0.57						
			13.79	**−1.22**	**0.57**	**0.003**	**0.564**	**0.570**	**36**	**35**	**37**

Table 3
Calculated $\delta^{18}O$ signatures of the calcite mineralizing fluid.

Location	Name	$\delta^{18}O_{fluid}$ ‰ (SMOW) (Kim and O'Neil, 1997)				
		1000ln(a)	a	$\delta^{18}O_{fluid}$ ‰ (SMOW)	$\delta^{18}O_{fluid}$ min	$\delta^{18}O_{fluid}$ max
Tournoux outcrop 1	FP18-2B	12.92	1.013	**−4.44**	−5.58	−3.27
	FP18-3A	11.99	1.012	**−2.92**	−3.49	−2.35
Tournoux outcrop 2	calcite cement	25.86	1.026	**−12.08**	−12.26	−11.91

4. Results

4.1. Petrology and microscopical analysis

The petrological microcrystalline structure of the hematite-rich samples from the Clarée and Tournoux sites were observed by optical and SEM imagery. Fig. 6 shows optical and SEM images of veins and striated hematite planes at both macro and micro scales in representative samples. The vein and fault plane samples taken from the Clarée site exhibit botryoidal aggregates and randomly oriented platy texture, whith a mean crystallite diameter of approximately 70 nm (from 40 to 110 nm). At the Tournoux site, the hematite samples from the fault exhibit clusters of hematite that are more or less botryoidal and approximately 2 μm in diameter (Fig. 6). The mean crystallite diameter is ∼ 40 nm (± 10 nm at 1σ, Supplementary Data 4). No variation in crystallite size was observed with increasing distance from the shear plane. Hematites observed on the shear plane are striated (Fig. 6). The hematite vein samples also exhibit a botryoidal texture and planar flakes without any preferential orientation. The mean hematite crystallite size in these samples is ∼ 68 nm, which is significantly larger than that of the fault hematite (Fig. 6).

4.2. Hematite (U–Th)/He data

In this study, 59 hematite (U-Th)/He measurements were obtained, 6 on sample aliquots from the Clarée site (three from veins and three from a striated fault plane) and 53 on the Tournoux site samples (12 from veins and 41 from the fault plane) (Supplementary Data 4). Fig. 7 shows H/He ages corrected for He loss as a function of mean crystallite size, Sm and effective uranium (eU) concentration (eU = [U] + 0.238 × [Th] + 0.0012 × [Sm]; Gastil et al., 1967). In the Tournoux site, hematites show a broad linear correlation between mean crystallite size and H/He age (Fig. 7). In addition, the Sm and eU concentrations (Supplementary Data 3) in the dated aliquots are in good agreement with the major and trace analyses (Fig. 7, Supplementary Data 2). The Clarée samples show H/He ages older than the Tournoux site samples and have lower Sm and eU values (Fig. 7, Supplementary Data 2). In detail, hematite vein and striated fault plan samples from the Clarée site show (U-Th)/He ages ranging from 13.3 ± 0.8 Ma to 8.9 ± 0.4 Ma and Sm and eU concentrations of 0.2–1.6 ppm and 1.0 − 2.2 ppm, respectively.

For the Tournoux site, vein H/He ages range from 1.9 ± 0.1 Ma to 1.0 ± 0.1 Ma, with Sm and eU concentrations of ∼ 1–2 and ∼ 3 − 5 ppm, respectively (Fig. 7). It is observed that for certain subsamples, aliquots exhibit homogeneous ages within an age uncertainty of 5% (Supplementary Data 4). The hematites found on the striated vein and fault plane exhibit younger ages compared to the veins. The age values range from 1.6 ± 0.2 Ma to 0.2 ± 0.1 Ma (except for one age at 1.6 ± 0.2 Ma, which seems to be an outlier, Fig. 7b). Additionally, they have higher Sm content (∼2 − 5 ppm) but similar eU concentration (∼2 − 5 ppm). Interestingly, the H/He age and Sm are negatively correlated for all Tournoux site hematite samples.

4.3. U-Pb calcite data

A new U-Pb age is presented for calcite from the Puy Chalvin site (see section 3.1.2). At thin-section scale, several generations of carbonates are identified (Fig. 8a). The first corresponds to dolomite crystals of several hundred micrometers diameter (dol 1 in Fig. 8). Although angular in places, this first generation of dolomite was partially replaced by a second generation of dusty-looking calcite (cal 2 in Fig. 8). In the cal 2 patches, crystals are small (<10 μm) and appear dark in cathodoluminescence. Clear growth zonings are observable in both small and large crystals under cathodoluminescence. The chronology of the carbonates is emphasized by the interplay between the growth zonations of dolomite, areas that have been replaced by calcite, and also by the observation of remobilized dolomite clast cemented by the cal 2 generation. A third generation (cal 3 in Fig. 8) is a clear sparitic calcite in plain polarized light, but appears zoned in cathodoluminescence. Only the last generation of calcite (cal 3) showed U-Pb ratios suitable for dating, and an age of 5.3 ± 0.6 Ma was obtained (Fig. 8b). This age corresponds to the breccia cementation, which is thus posterior to the fault movement.

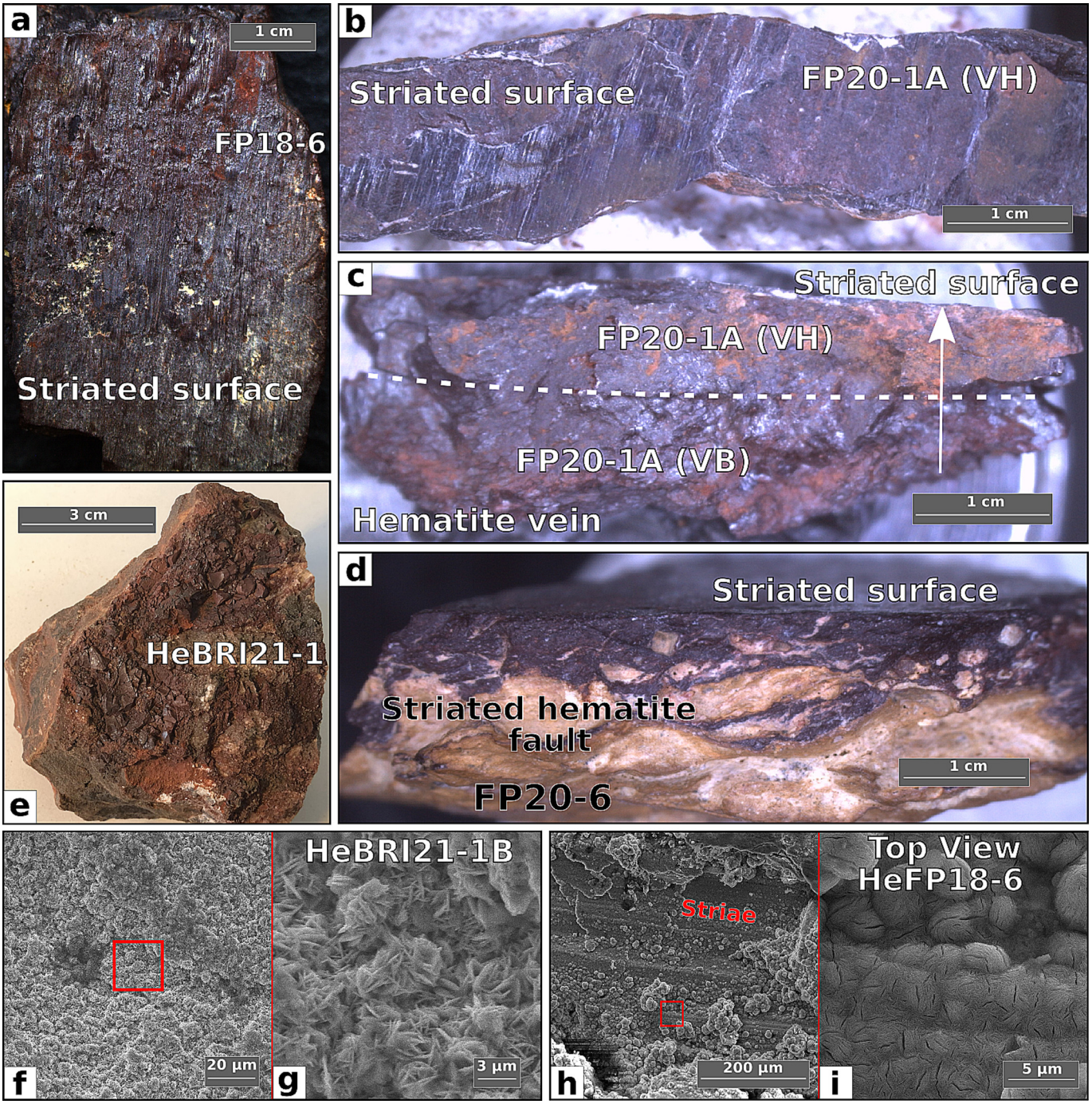

Fig. 6. Representative optical photographs of hematite samples (a, b, plane surface and c, d, perpendicular to the striated plane), of millimetric vein hematite samples (e). (f-i) SEM images showing textural relationships along the striae, where botryoidal crystallization of hematite has occured.

4.4. Stable isotope results

A significant difference in Δ_{47} temperature was obtained between samples from the western Tournoux outcrop 1 (~130 °C) and eastern Tournoux outcrop 2 (~36 °C, Table 2). Assuming that these temperatures correspond to the crystallization temperature, the signature of the mineralizing fluid was calculated using the water-calcite fractionation equations (Kim and O'Neil, 1997). A distinct fluid signature was obtained in calcites from the western ($\delta^{18}O_{fluid}$ = −2.4‰ to −5.6‰ in outcrop 1) and eastern ($\delta^{18}O_{fluid}$ = −11.9‰ to −12.3‰ in outcrop 2) parts of Tournoux site (Table 3).

5. Discussion

5.1. Relationships between fluid and fault activity

Several studies have traced the evolution of near-surface conditions in mountain belts through the study of fluid-rock interaction using stable isotopes (Campani et al., 2012; Krsnik et al., 2021; Cardello et al., 2024). At the Tournoux site, the evolution of the extensional fault network resulted in the reactivation of the PFT between 3.6 and 0.5 Ma (based on U-Pb ages from Bilau et al. (2021) and H/He ages from this study). During this extensional

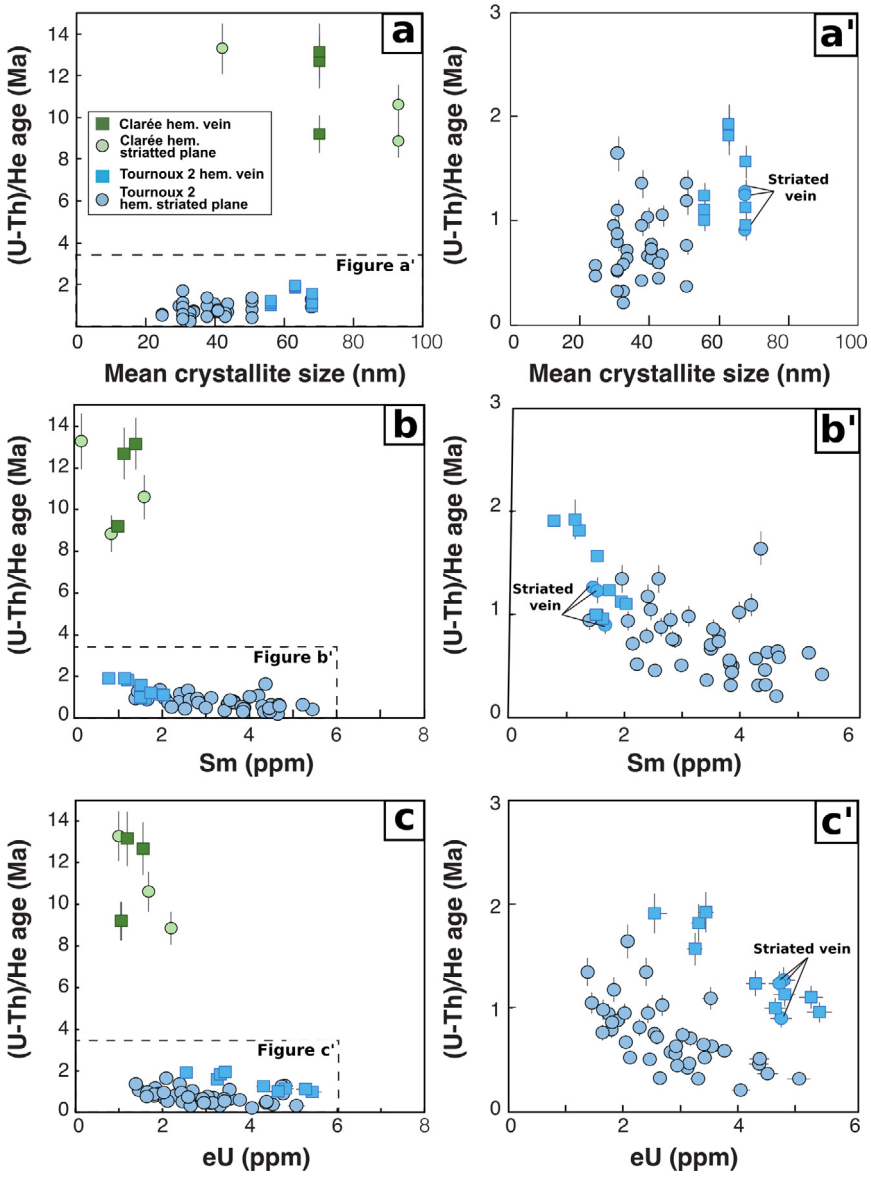

Fig. 7. Relationship of (U-Th)/He ages with respect to mean crystallize size (a), Sm concentration (b) and effective Uranium concentration eU (c) for the striated hematite veins for both the Clarée and the Tournoux outcrop 2. A close-up of the lower part of each figure is presented in a', b' and c' to highlight the relationship within the Tournoux outcrop 2 data.

fault event, two stages of fluid circulation are evidenced. The clumped isotope results show that the 3.4–2.3 Ma calcite breccia (Tournoux outcrop 1, Fig. 5) corresponds to a fluid temperature > 110 °C (115–138 °C, Table 2) and $\delta^{13}C_{calcite}$ values in agreement with a highly heated meteoric source (Fig. 9, Bilau et al., 2021). A nearby AFT age of 25 Ma (Tricart et al., 2007) indicates that the temperature since that time was below ~ 90 °C, corresponding to the closure temperature of the AFT (Reiners and Brandon, 2006). This suggests that the 3 Ma old fluids were in disequilibrium with the surrounding host rocks. The Δ_{47} temperature of 115 − 138 °C is interpreted as the crystallization temperature of the calcites during this stage of hot fluid circulation. Given an exhumation rate of 1 mm·yr^{-1} (Tricart et al., 2007; Girault et al., 2022), and the calcite U-Pb age (Bilau et al., 2021), calcite crystallization must have occurred at a depth < 3.5 km. The stable isotopic composition of these > 110 °C Tournoux site fluids (−4‰ SMOW) differs significantly from the signature of Alpine thermal sources (−10‰ to −15‰ SMOW, Figs. 9 and 10), and is inconsistent with the $\delta^{18}O$ gradient with elevation observed for meteoric water in the area (Fig. 10).

In contrast, the calcite from the fault breccia at Tournoux outcrop 2, crosscut by the ca. 2 Ma hematite, has a lower crystallization temperature of approximately 36 °C and exhibits a different fluid signature of −12‰ (SMOW). This signature is similar to that obtained for waters from thermal sources in the W-Alps (Poulain, 1977; Blavoux et al., 1982) and corresponds to meteoric fluids that seeped down and interacted to varying degrees with the surrounding rocks. The $\delta^{18}O$ signatures of the fluids can infer precipitation elevations (Campani et al., 2012) although they also reflect interactions with surrounding rocks (Chamberlain and Poage, 2000; Poage and Chamberlain, 2001). According to Poulain (1977), the hydrothermal spring waters within the Briançonnais are likely derived from meteoric waters that were precipitated at an elevation of approximately 1900 m. This elevation corresponds to the average relief of the mountain peaks that surround the Durance valley (Fig. 10). Fluids are therefore interpreted as having a mete-

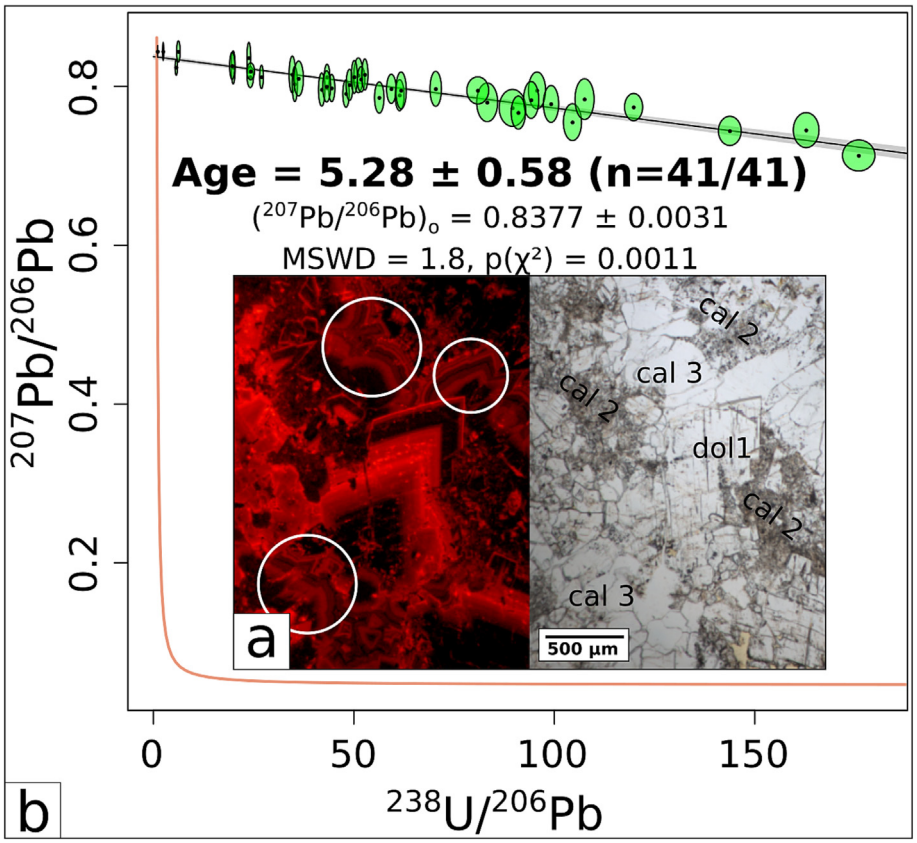

Fig. 8. U-Pb age data and microscopic images of calcite from the cataclasite sample of the Puy Chalvin site. (a) Single polarized light (right) and cathodoluminescence (left) images identifying the three generations of carbonates; white circles mark areas where spots were placed during analysis. (b) Tera-Wasserburg diagram, showing the isochron correlation with statistical indicators (Mean Square Weighted Deviation, MSWD and chi-square, χ^2) related to the number of spots (n).

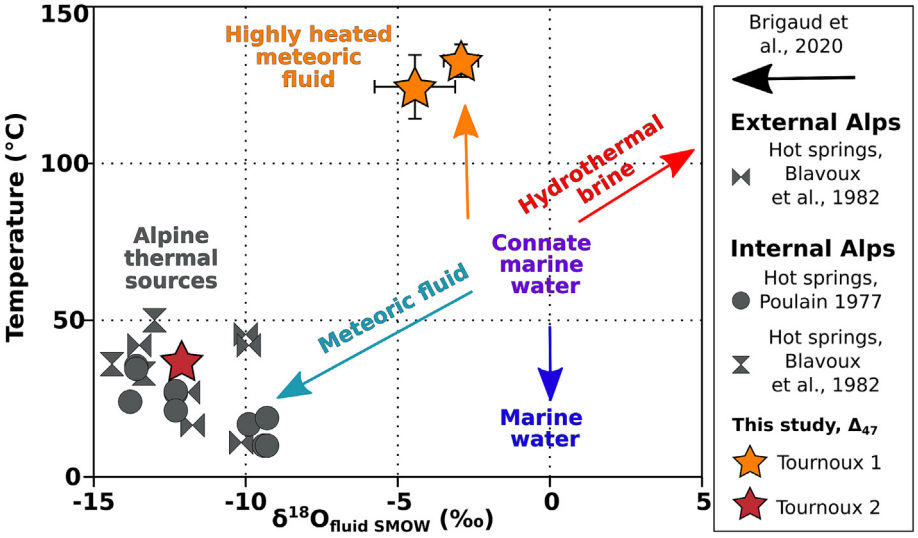

Fig. 9. Calculated crystallization temperatures based on Δ_{47} data as a function of the calculated isotopic fluid signature (Kim and O'Neil, 1997) of the studied High-Durance Fault System compared to data from Western Alps hot springs. Dark grey data correspond to results from thermal spring samples in the internal and external Alps (Poulain, 1977; Blavoux et al., 1982). The trends (marked by arrows) are taken from Brigaud et al. (2020) except for the orange arrow, which is based on the data of this study. (For interpretation of the references to color in this figure legend, the reader is referred to the web version of this article.)

oric origin coming from an elevation close to ~ 1700 m, similar to that at which the samples were collected. This indicates that the elevation of the meteoric seepage zones above the sampled active fault was similar to the present day topography during paleofluid circulation 2 Ma ago. The temperature of ~ 36°C suggests that the meteoric fluids circulated down to a depth of 1–2 km and ascended back to the valley bottom.

In summary, two main fluid regimes are identified through time and depth within the Tournoux study area, including (1) deep and hot hydrothermal fluids (>110 °C) that flowed upward between ca.

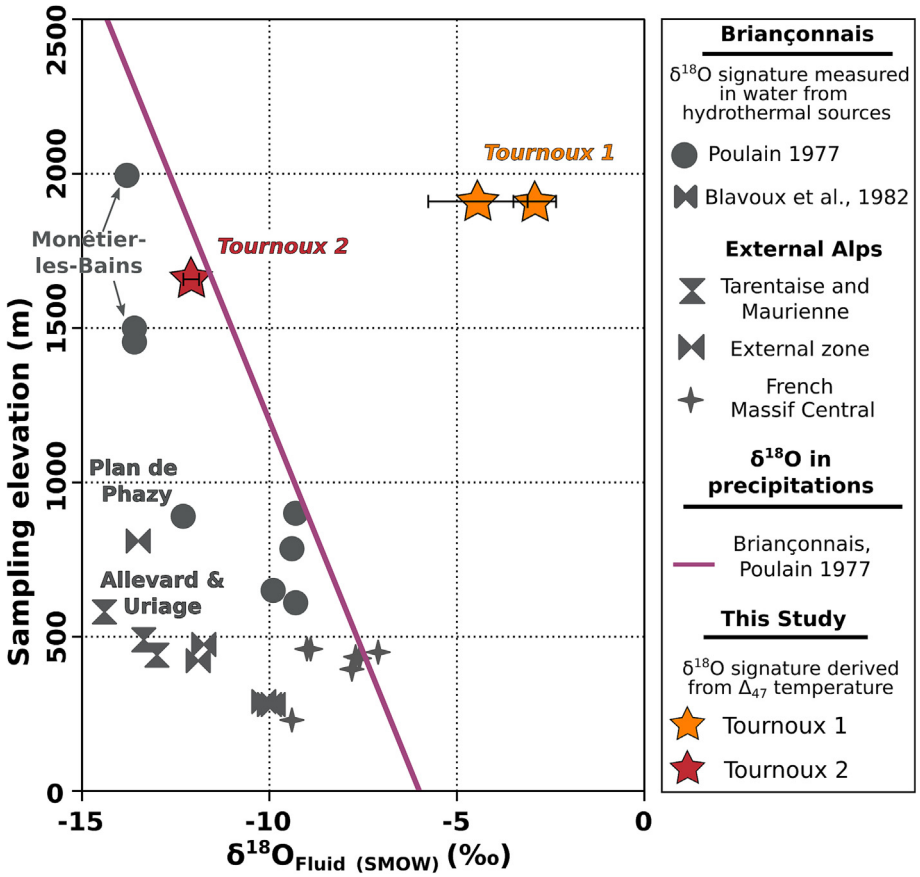

Fig. 10. Isotopic $\delta^{18}O$ fluid compositions from the studied fault zones (red and orange stars, calculated from the Δ_{47} of the sampled calcites) and hydrothermal (dark grey, taken from springs Poulain, 1977; Blavoux et al., 1982) as well as meteoritic waters in the study area plotted against sampling altitude. The purple curve corresponds to water composition from rainfalls at different altitudes in the Western Alps. (For interpretation of the references to color in this figure legend, the reader is referred to the web version of this article.)

3.6 Ma and 2 Ma, and (2) shallow fluids associated with the downward infiltration of meteoric water since 2 Ma. The abrupt change at 2 Ma may have corresponded to the time when glacial erosion isolated the upper part of the fault due to the lowering of the valley bottom.

5.2. Significance of hematite ages for the tectonic evolution of the Briançonnais zone

In both sites dated with the H/He method, hematites precipitate from low temperature fluids of meteoric origin, which crystallized during fault activity. For the Tournoux site, fluids have precipitated at a temperature below 36 ± 1 °C. This temperature is lower than the He closure temperature of 70–90 °C for hematite crystallites of 30 to 90 nm (Balout et al., 2017; Farley, 2018). Consequently, the H/He ages obtained in this study are interpreted as crystallization ages. The estimated crystallization depth is of ~ 1 km, based on a thermal gradient of 30 °C/km. For the Clarée site, the hematite crystallization temperature is not known, but it is assumed to lie below the temperature sentivity of the H/He system. This hypothesis is supported by the AFT data (Tricart et al., 2007), which indicate that temperatures have remained below 90 °C since 31 – 22 Ma in this region. These low temperature conditions at both sites are not sufficient to induce a reopening of the H/He system, so these ages can be interpreted as associated with fault activity (McDermott et al., 2017, 2021; Ault et al., 2019a; Ault, 2020).

For the Clarée site to the east of the Briançonnais zone (see section 3.1.1) the youngest obtained age (ca. 8 Ma) is from a hematite vein without any brittle deformation feature (e.g., striae), which is unsuggestive of any frictional heating (as defined by Ault et al., 2019a, b; Calzolari et al., 2020). We thus favor the hypothesis of a more or less continuous fault activity between ca. 13 Ma and 8 Ma, which led to incremental vein opening and hematite crystallization. In the Tournoux site (Fig. 6f–i) petrological observations highlight several generations of hematite, which crystallized during incremental fault activity. It follows, from our two study sites, that (U-Th)/He hematite ages should be interpreted as crystallization ages in close relationship to fault slip events, during which the hematite may have crystallized or been reset. The source of the H/He ages dispersion could be due to overheating even at temperature of 600 °C as pointed by Danišík et al. (2013) or to U-Th or Sm concentrations that evolved during the precipitation of hematite in the vein and striated hematite.

The onset of hematite precipitation at the Clarée site could be older than ca. 13 Ma and could have lasted for some Myrs. Based on field work observations, it is concluded that the studied paleokarst was formed during the Cenozoic after nappe stacking in the Alps (Mercier, 1977; Barféty et al., 1996). Based on the 13 Ma minimum age for extensional fault activity in the area, the age of karst formation must be older than 13 Ma.

To the west of the Briançonnais zone (Tournoux site) the vein filled with the first hematite generation shows a H/He age range from ca. 2 Ma to 1 Ma (Fig. 7). H/He ages decrease with increasing Sm and eU concentrations, which can be interpreted as the chemical evolution of the mineralizing fluid from 2 Ma to 1 Ma (Fig. 7). In the same location, mm-scale hematite precipitated in the veins

and the hematite fault plane coatings are striated (Fig. 6). The final movements led to the striation of the hematite fault plane and thus the reset of the H/He system at around 1 Ma. The first precipitation of fault plane hematite is recorded at ca. 1.6 Ma, with a Sm content similar to the striated vein that could indicate a similar common mineralizing fluid for the vein and the coated hematite fault plane. However, the first precipitated hematites along the faut planes are characterized by low eU (1.5–2 ppm), while the youngest hematite samples show an increase of the eU content up to 5 ppm at 0.2–0.4 Ma (Fig. 7c). This increase in eU and Sm contents is interpreted as reflecting the evolution of the parent fluid.

Despite a similar exhumation context (based on similar AFT ages, Seward et al., 1999; Tricart et al., 2007) for the two sites studied in the Briançonnais zone, both in the hanging wall of the PFT, the H/He ages obtained here are significantly different and show an east–west diachronism. Ages of 13.3 ± 0.8 Ma to 8.9 ± 0.4 Ma are obtained along the CFZ to the east of the Briançonnais zone, while ages of 1.9 ± 0.1 Ma to < 0.8 Ma are obtained at the Tournoux site, to the west of the Briançonnais zone. Furthermore, while the H/He ages from the CFZ are only slightly younger than the AFT ages from the same unit (Seward et al., 1999; Tricart et al., 2007), the H/He ages from Tournoux site are much younger (<2 Ma), even younger than the U-Pb on calcite ages obtained this site (2–4 Ma). The hematite (U-Th)/He and calcite U-Pb ages from this study (Fig. 11) suggest a westward propagation of transtensional fault activity in the Briançonnais zone, from ca. 13 Ma in the east (CFZ), ca. 5 Ma in the centre (Puy-Chalvin site) to ca. 4 Ma to < 0.8 Ma in the west (HDZ). The ages also indicate that the Briançonnais zone underwent a phase of karstification before 13 Ma, and that this area has undergone little erosion and exhumation since. It follows that the Briançonnais zone remained in a steady state topographic equilibrium for a long time, until the onset of the glaciations in the Quaternary.

5.3. Implications for the Western Alps tectonic evolution

The occurrence of extension in the core of the Alpine collisional belt has been interpreted as an example of gravity collapse (e.g., Selverstone, 2005), following a supposedly pure compressional context (Royden and Burchfiel, 1989). This assertion has been supported by the observation of extensional reactivation of major thrusts (e.g., Sue et al., 2007), and relatively young ages obtained for this reactivation (4–2 Ma, Bilau et al., 2021). However, as pointed out in the previous section, the onset of extension probably occurred much earlier. Our study suggests a westward propagation of extensional fault activity in the Briançonnais zone, from 13 Ma to < 2 Ma. Results suggest that extension activity coincided with compression at the front of the chain of the Western Alps (Fig. 12). Westward propagation of the frontal fold and thrust belt into the European foreland is bracketed between 15 Ma and 8 Ma for the subalpine massifs (Bilau et al., 2023a) and between 14.3 Ma and 4.5 Ma for the Jura mountains (Looser et al., 2021; Smeraglia et al., 2021). Rooting of thrusts below the ECMs allowed their exhumation since around 22 Ma with an acceleration at 10–8 Ma (Beucher et al., 2012; Boutoux et al., 2016; Girault et al., 2022; Lemot et al., 2023). Therefore, we interpret the extension occurring in the Briançonnais zone as a relative down throw motion at the back of the ECMs. Uplift of ECMs is related to thrusting on a crustal-scale ramp, corresponding to the Alpine Frontal Thrust rooting down below the ECMs and propagates westward at the cover-basement interface of the Alpine foreland (Bellahsen et al., 2014; Schwartz et al., 2017, 2024; Rolland et al., 2022, Fig. 12). The combination of recent S-wave tomography (Nouibat et al., 2022) and stress regime inversion (Mathey et al., 2022) suggests that extensional activity in the internal Alps was likely caused by the decoupling of the Adriatic mantle indentor into two main units (Schwartz et al., 2024). The upper part of the rigid mantle designated the Adria Seismic Body (ASB, Fig. 12) is responsible for the shortening of the South Alpine crust and the vertical indentation of the subduction wedge. The uplift of the ASB is indicated by a Moho depth shallower than 10 km. Active extension highlighted in the seismicity is localized at the boundary of the extruding HP wedge of the internal Alps exhumed by the ASB (Schwartz et al., 2024).

Based on our new geochronological constraints, we propose that the period between 16 Ma (older ages of the fold-and-thrust belt activity, Bilau et al., 2023a) and 13 Ma (minimum H/He age for the initiation of extension in the High Durance Fault System) was a transitional stage in the evolution of the orogenic wedge of the Western Alps. During this period, there was a transition from compressive to extensive stress regimes in the internal zones (Briançonnais and Piedmont zones) and the development of a compressive regime in the external zones (ECMs and European foreland, Bilau et al., 2023a). This compression is suggested to be repsonsible for activating the Alpine Frontal Thrust, exhuming the ECMs and developing a fold and thrust belt in the foreland. In this context, the Briançonnais zone, situated behind the PFT exhibits a relative downthrow motion, thereby facilitating the development of the High-Durance Fault System (especially HDZ and CFZ) in conjunction with the extensional reactivation of the PFT. The concomitant occurrence of compressive and extensive regimes, and their parallel westward propagation on both sides of the ECMs, permit the proposition that extension in the Western Alps is not solely based on post-collisional tectonic collapse, or to any enhanced erosional processes (e.g., Cederbom et al., 2004; Champagnac et al., 2007). It can thus be proposed that convergence *syn*-orogenic extension should be considered as an important process, in response to a global shortening of the chain and linked to anticlockwise rotation of the Adriatic plate. The development of the extension is synchronous with the propagation of the frontal

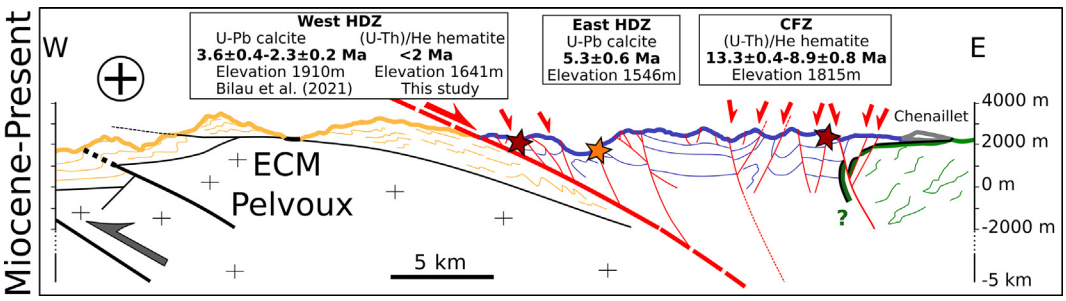

Fig. 11. Tectonic cross-section of the Briançonnais zone with the ages of fault activity (modified from Bilau et al., 2021). Yellow line correspond to the external sedimentary cover, blue line corresponds to the Briançonnais zone, green line corresponds to the Piedmont zone and the grey line corresponds to the Chenaillet unit with the main fault zones, High-Durance Zone (HDZ) and the Clarée Fault Zone (CFZ). U-Pb ages are given with 2σ error while (U-Th)/He ages are given with 1σ error. (For interpretation of the references to color in this figure legend, the reader is referred to the web version of this article.)

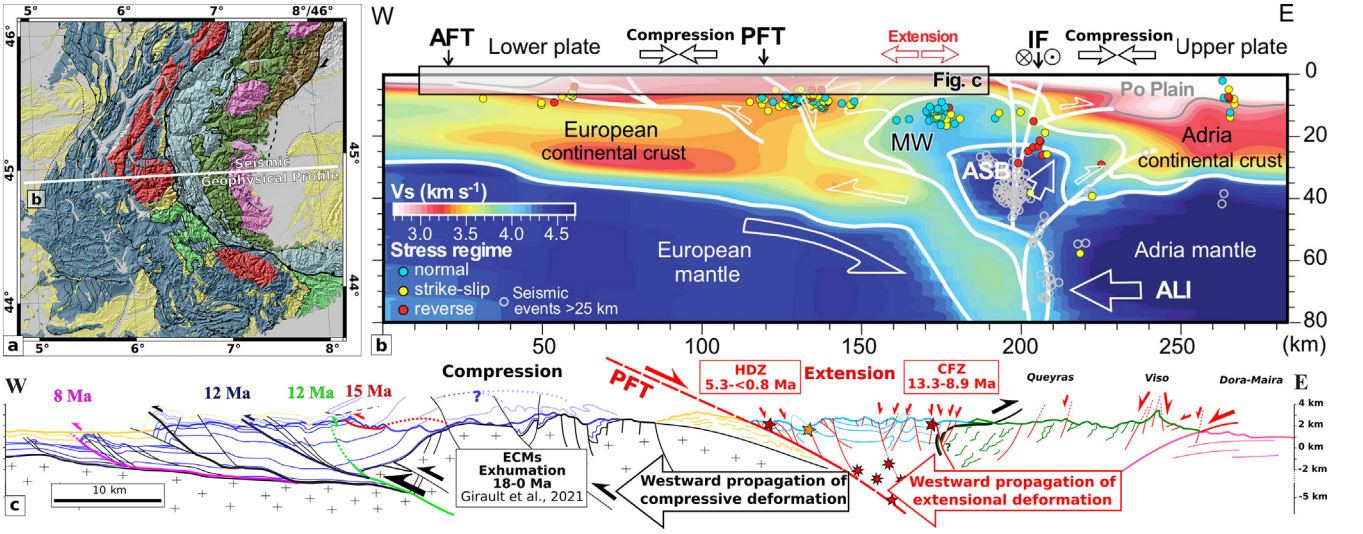

Fig. 12. (a) Tectonic map of the Western Alps with position of the cross-sections (same legend as in Fig. 1). (b) Seismic geophysical profile showing interpretations of geological structure boundaries, Alpine Frontal Thrust (AFT), Penninic Frontal Thrust (PFT), Insubric Fault (IF), Adria Seismic Body (ASB), Adria Lithospheric Mantle (ALI), Mantle Wedge (MW) based on the Vs velocity model from Nouibat et al. (2022) and Schwartz et al. (2024). (c) Tectonic cross-section of the Western Alps. The geometry of the Alpine foreland (west of Penninic Frontal Thrust, PFT) is drawn after Bellahsen et al. (2014), Kalifi et al. (2021), and Bilau et al. (2023a). The internal Alps (east of PFT) are taken from Tricart et al. (2006) and Bilau et al. (2021). For lithologies legend, refer to Fig. 1 caption except that External Crystalline Massifs (ECMs) basement is in black. Ages of High-Durance Fault System extensional fault activity (determined by U-Pb calcite and (U-Th)/He on hematite) are shown in red rectangles, while exhumation of ECMs constrained by Apatie Fission Track ages is shown in a black rectangle. Ages of main foreland belt thrust faults indicated by roman letters are U-Pb ages on calcite of fault increments from Bilau et al. (2023a). (For interpretation of the references to color in this figure legend, the reader is referred to the web version of this article.)

thrust structures in the sedimentary cover and to the crustal stacking of the European crust below the ECMs. This tectonic context remains active, as evidenced by the distribution of the strain field, in relation to the Adriatic mantle indentor (Schwartz et al., 2024).

6. Conclusions

The combination of crystallisation ages obtained through the use of hematite (U-Th)/He and calcite U-Pb dating, in conjunction with the isotopic signatures ($\delta^{13}C$, $\delta^{18}O$, and Δ_{47}) of the fluids related to calcite allows to pin-point the history of fluid-rock interaction in an evolving tectonic and geomorphological framework. Stable isotope analysis has revealed a transition in the fluid regimes flowing through the extensional faults over the past three million years, as recorded in calcite precipitated along the fault. The first regime, which prevailed before 2 Ma, is associated with upwelling of deep hydrothermal fluids with $T > 110$ °C. The second fluid regime, since 2 Ma, is characterised by a meteoritic signature and much lower temperatures of around 36 °C. This transition is interpreted as the result of valley incision in response to the Quaternary glacial phases.

The east–west progression of hematite and calcite ages allows the formulation of a new model for the comprehension and evolution of Alpine *syn*-orogenic extension. The onset of extension, as determined by helium ages on hematite, is estimated to have occurred at a minium age of 13 Ma to the east of the Briançonnais zone (CFZ). The propagation of extension proceeded in a westerly direction, reaching the center of the Briançonnais zone at ca. 5 Ma and ultimately its western margin (HDZ) at 3 Ma. The extension observed within the Briançonnais zone is linked to the extensional reactivation of the PFT and is synchronous with the development of the Alpine foreland, since 16 Ma. The Alpine Frontal Thrust plays a pivotal role in the tectonic evolution of the region, as its involvement serves to facilitate the exhumation of the ECMs. The development of the High-Durance Fault System, at rear back of ECMs, is here considered as the accommodation of ECMs exhumation. It can thus be concluded that this *syn*-convergent orogenic extension, which is associated with the development of the collisional structures, is not linked to post-orogenic processes such as post-collisional tectonic collapse but is controlled by mantle indentation during anticlockwise rotation of the Adriatic plate.

CRediT authorship contribution statement

Antonin Bilau: Writing – review & editing, Writing – original draft, Project administration, Methodology, Investigation, Formal analysis, Data curation, Conceptualization. **Yann Rolland:** Writing – review & editing, Writing – original draft, Visualization, Validation, Supervision, Project administration, Investigation, Funding acquisition, Conceptualization. **Stéphane Schwartz:** Writing – review & editing, Visualization, Validation, Supervision, Investigation, Funding acquisition, Conceptualization. **Cécile Gautheron:** Writing – review & editing, Validation, Supervision, Methodology, Investigation, Formal analysis, Data curation. **Thierry Dumont:** Writing – review & editing, Visualization, Validation, Supervision, Investigation, Conceptualization. **Dorian Bienveignant:** Investigation. **Benjamin Brigaud:** Writing – review & editing, Validation, Supervision, Methodology, Data curation. **Nicolas Godeau:** Validation, Supervision, Methodology, Formal analysis, Data curation. **Abel Guihou:** Writing – review & editing, Validation, Supervision, Methodology, Data curation. **Pierre Deschamps:** Writing – review & editing, Funding acquisition. **Xavier Mangenot:** Formal analysis, Data curation. **Marianna Corre:** Formal analysis, Data curation. **Rosella Pinna-Jamme:** Formal analysis, Data curation. **Nathaniel Findling:** Formal analysis, Data curation.

Declaration of competing interest

The authors declare that they have no known competing financial interests or personal relationships that could have appeared to influence the work reported in this paper.

Acknowledgments

This work forms part of the first author's Ph.D. project funded by the French BRGM in the frame of the RGF-Alps program (Référentiel Géologique de la France). The LA-ICP-MS hosted by the ENVITOP platform at CEREGE has received funding from the "Excellence Initiative" of the Aix Marseille University A*MIDEX – project DATCARB, a french "Investissement d'avenir" program. Special thanks to Fayçal Soufi and Pierre-Luigi Canepa for their preparation of polished thin-section. The authors thank the reviewers, Meinert Rahn and Martin Danišík, for their careful reading and insightful comments, and efficient editorial handling by Stijn Glorie (Associate Editor) and M. Santosh (Editorial Advisor), which greatly helped to improve this manuscript.

Appendix A. Supplementary data

Supplementary data to this article can be found online at https://doi.org/10.1016/j.gsf.2024.101969.

References

Allard, T., Gautheron, C., Bressan Riffel, S., Balan, E., Soares, B.F., Pinna-Jamme, R., Derycke, A., Morin, G., Bueno, G.T., do Nascimento, N., 2018. Combined dating of goethites and kaolinites from ferruginous duricrusts. Deciphering the Late Neogene erosion history of Central Amazonia. Chem. Geol. 479, 136–150. https://doi.org/10.1016/j.chemgeo.2018.01.004.

Ault, A.K., 2020. Hematite fault rock thermochronometry and textures inform fault zone processes. J. Struct. Geol. 133, 104002. https://doi.org/10.1016/j.jsg.2020.104002.

Ault, A.K., Gautheron, C., King, G.E., 2019a. Innovations in (U–Th)/He, fission track, and trapped charge thermochronometry with applications to earthquakes, weathering, surface-mantle connections, and the growth and decay of mountains. Tectonics 38, 3705–3739. https://doi.org/10.1029/2018TC005312.

Ault, A.K., Jensen, J.L., McDermott, R.G., Shen, F.-A., Van Devener, B.R., 2019b. Nanoscale evidence for temperature-induced transient rheology and postseismic fault healing. Geology 47, 1203–1207. https://doi.org/10.1130/G46317.1.

Balout, H., Roques, J., Gautheron, C., Tassan-Got, L., Mbongo-Djimbi, D., 2017. Helium diffusion in pure hematite (α-Fe_2O_3) for thermochronometric applications: a theoretical multi-scale study. Comput. Theor. Chem. 1099, 21–28. https://doi.org/10.1016/j.comptc.2016.11.001.

Barféty, J.-C., Lemoine, M., De Graciansky, P.-C., Tricart, P., Mercier, D., 1996. Notice explicative de la carte géologique de la France à 1/50 000. 823, Briançon. Bureau de recherches géologiques et minières, Orléans.

Bauve, V., Plateaux, R., Rolland, Y., Sanchez, G., Bethoux, N., Delouis, B., Darnault, R., 2014. Long-lasting transcurrent tectonics in SW Alps evidenced by Neogene to present-day stress fields. Tectonophysics 621, 85–100.

Beaudoin, N., Lacombe, O., Roberts, N.M.W., Koehn, D., 2018. U-Pb dating of calcite veins reveals complex stress evolution and thrust sequence in the Bighorn Basin, Wyoming, USA. Geology 46, 1015–1018. https://doi.org/10.1130/G45379.1.

Bellahsen, N., Mouthereau, F., Boutoux, A., Bellanger, M., Lacombe, O., Jolivet, L., Rolland, Y., 2014. Collision kinematics in the western external Alps. Tectonics 33, 1055–1088.

Bellanger, M., Augier, R., Bellahsen, N., Jolivet, L., Monié, P., Baudin, T., Beyssac, O., 2015. Shortening of the European Dauphinois margin (Oisans Massif, Western Alps): new insights from RSCM maximum temperature estimates and $^{40}Ar/^{39}Ar$ in situ dating. J. Geodyn. 83, 37–64. https://doi.org/10.1016/j.jog.2014.09.004.

Beucher, R., van der Beek, P., Braun, J., Batt, G.E., 2012. Exhumation and relief development in the Pelvoux and Dora-Maira massifs (Western Alps) assessed by spectral analysis and inversion of thermochronological age transects. J. Geophys. Res. Earth Surf. 117, F03030.

Bilau, A., Rolland, Y., Dumont, T., Schwartz, S., Godeau, N., Guihou, A., Deschamps, P., 2023b. Early onset of Pyrenean collision (97–90 Ma) evidenced by U-Pb dating on calcite (Provence, SE France). Terra Nova 35 (5), 413–423. https://doi.org/10.1111/ter.12665.

Bilau, A., Bienveignant, D., Rolland, Y., Schwartz, S., Godeau, N., Guihou, A., Deschamps, P., Mangenot, X., Brigaud, B., Boschetti, L., Dumont, T., 2023a. The Tertiary structuration of the Western Subalpine foreland deciphered by calcite-filled faults and veins. Earth-Sci. Rev. 236, 104270. https://doi.org/10.1016/j.earscirev.2022.104270.

Bilau, A., Rolland, Y., Schwartz, S., Godeau, N., Guihou, A., Deschamps, P., Brigaud, B., Noret, A., Dumont, T., Gautheron, C., 2021. Extensional reactivation of the Penninic frontal thrust 3 Myr ago as evidenced by U-Pb dating on calcite in fault zone cataclasite. Solid Earth 12, 237–251. https://doi.org/10.5194/se-12-237-2021.

Blavoux, B., Dazy, J., Sarrot-Reynauld, J., 1982. Information about the origin of thermomineral waters and gas by means of environmental isotopes in eastern Azerbaijan, Iran, and southeast France. J. Hydrol. 56, 23–38. https://doi.org/10.1016/0022-1694(82)90054-3.

Bonifacie, M., Calmels, D., Eiler, J.M., Horita, J., Chaduteau, C., Vasconcelos, C., Agrinier, P., Katz, A., Passey, B.H., Ferry, J.M., Bourrand, J.-J., 2017. Calibration of the dolomite clumped isotope thermometer from 25 to 350 °C, and implications for a universal calibration for all (Ca, Mg, Fe)CO_3 carbonates. Geochim. Cosmochim. Acta 200, 255–279. https://doi.org/10.1016/j.gca.2016.11.028.

Boutoux, A., Bellahsen, N., Nanni, U., Pik, R., Verlaguet, A., Rolland, Y., Lacombe, O., 2016. Thermal and structural evolution of the external Western Alps: Insights from (U–Th–Sm)/He thermochronology and RSCM thermometry in the Aiguilles Rouges/Mont Blanc massifs. Tectonophysics 683, 109–123.

Brigaud, B., Bonifacie, M., Pagel, M., Blaise, T., Calmels, D., Haurine, F., Landrein, P., 2020. Past hot fluid flows in limestones detected by Δ_{47}–(U-Pb) and not recorded by other geothermometers. Geology 48, 851–856. https://doi.org/10.1130/G47358.1.

Brigaud, B., Andrieu, S., Blaise, T., Haurine, F., Barbarand, J., 2021. Calcite uranium–lead geochronology applied to hardground lithification and sequence boundary dating. Sedimentology 68, 168–195. https://doi.org/10.1111/sed.12795.

Calzolari, G., Ault, A.K., Hirth, G., McDermott, R.G., 2020. Hematite (U-Th)/He thermochronometry detects asperity flash heating during laboratory earthquakes. Geology 48, 514–518. https://doi.org/10.1130/G46965.1.

Campani, M., Mulch, A., Kempf, O., Schlunegger, F., Mancktelow, N., 2012. Miocene paleotopography of the Central Alps. Earth Planet. Sci. Lett. 337–338, 174–185. https://doi.org/10.1016/j.epsl.2012.05.017.

Cardello, G.L., Bernasconi, S.M., Fellin, M.G., Rahn, M., Rosskopf, R., Maden, C., Mancktelow, N.S., 2024. Carbonate deformation through the brittle-ductile transition: the case of the SW Helvetic nappes, Switzerland. J. Struct. Geol. 181, 105083. https://doi.org/10.1016/j.jsg.2024.105083.

Cederbom, C.E., Sinclair, H.D., Schlunegger, F., Rahn, M.K., 2004. Climate-induced rebound and exhumation of the European Alps. Geology 32, 709–712.

Cenki-Tok, B., Darling, J.R., Rolland, Y., Dhuime, B., Storey, C.D., 2014. Direct dating of mid-crustal shear zones with synkinematic allanite: new *in situ* U-Th-Pb geochronological approaches applied to the Mont Blanc massif. Terra Nova 26, 29–37. https://doi.org/10.1111/ter.12066.

Ceriani, S., Schmid, S.M., 2004. From NS collision to WNW-directed post-collisional thrusting and folding: structural study of the Frontal Penninic Units in Savoie (Western Alps, France). Eclogae Geol. Helvetiae 97, 347–369.

Ceriani, S., Fügenschuh, B., Schmid, S.M., 2001. Multi-stage thrusting at the" Penninic Front" in the Western Alps between Mont Blanc and Pelvoux massifs. Int. J. Earth Sci. 90, 685–702.

Chamberlain, C.P., Poage, M.A., 2000. Reconstructing the paleotopography of mountain belts from the isotopic composition of authigenic minerals. Geology 28, 115–118. https://doi.org/10.1130/0091-7613(2000)28<115:RTPOMB>2.0.CO;2.

Champagnac, J.D., Molnar, P., Anderson, R.S., Sue, C., Delacou, B., 2007. Quaternary erosion-induced isostatic rebound in the western Alps. Geology 35, 195–198.

Danišík, M., Evans, N.J., Ramanaidou, E.R., McDonald, B.J., Mayers, C., McInnes, B.I.A., 2013. (U–Th)/He chronology of the Robe River channel iron deposits, Hamersley Province, Western Australia. Chem. Geol. 354, 150–162. https://doi.org/10.1016/j.chemgeo.2013.06.012.

Dennis, K.J., Affek, H.P., Passey, B.H., Schrag, D.P., Eiler, J.M., 2011. Defining an absolute reference frame for 'clumped' isotope studies of CO_2. Geochim. Cosmochim. Acta 75, 7117–7131. https://doi.org/10.1016/j.gca.2011.09.025.

Dumont, T., Schwartz, S., Guillot, S., Simon-Labric, T., Tricart, P., Jourdan, S., 2012. Structural and sedimentary records of the Oligocene revolution in the Western Alpine arc. J. Geodyn. 56, 18–38.

Dumont, T., Schwartz, S., Guillot, S., Malusà, M., Jouvent, M., Monié, P., Verly, A., 2022. Cross-propagation of the western Alpine orogen from early to late deformation stages: evidence from the Internal Zones and implications for restoration. Earth-Sci. Rev. 232, 104106. https://doi.org/10.1016/j.earscirev.2022.104106.

Evenson, N.S., Reiners, P.W., Spencer, J.E., Shuster, D.L., 2014. Hematite and Mn oxide (U-Th)/He dates from the Buckskin-Rawhide detachment system, western Arizona: gaining insights into hematite (U-Th)/He systematics. Am. J. Sci. 314, 1373–1435. https://doi.org/10.2475/10.2014.01.

Farley, K.A., 2018. Helium diffusion parameters of hematite from a single-diffusion-domain crystal. Geochim. Cosmochim. Acta 231, 117–129. https://doi.org/10.1016/j.gca.2018.04.005.

Frey, M., Ferreiro Mählmann, R., 1999. Alpine metamorphism of the Central Alps. Schweizerische mineralogische und petrographische. Mitteilungen 79, 135–154.

Gastil, R.G., Delisle, M., Morgan, J., 1967. Some effects of progressive metamorphism on zircons. Geol. Soc. Am. Bull. 78, 879. https://doi.org/10.1130/0016-7606(1967)78[879:SEOPMO]2.0.CO;2.

Gautheron, C., Pinna-Jamme, R., Derycke, A., Ahadi, F., Sanchez, C., Haurine, F., Monvoisin, G., Barbosa, D., Delpech, G., Maltese, J., Sarda, P., Tassan-Got, L., 2021. Technical note: analytical protocols and performance for apatite and zircon (U–Th)/He analysis on quadrupole and magnetic sector mass spectrometer systems between 2007 and 2020. Geochronology 3, 351–370. https://doi.org/10.5194/gchron-3-351-2021.

Girault, J.B., Bellahsen, N., Bernet, M., Pik, R., Loget, N., Lasseur, E., Rosenberg, C.L., Balvay, M., Sonnet, M., 2022. Exhumation of the Western Alpine collisional wedge: new thermochronological data. Tectonophysics 822, 229155. https://doi.org/10.1016/j.tecto.2021.229155.

Heller, B.M., Riffel, S.B., Allard, T., Morin, G., Roig, J.-Y., Couëffé, R., Aertgeerts, G., Derycke, A., Ansart, C., Pinna-Jamme, R., Gautheron, C., 2022. Reading the climate signals hidden in bauxite. Geochim. Cosmochim. Acta 323, 40–73. https://doi.org/10.1016/j.gca.2022.02.017.

Hofmann, F., Treffkorn, J., Farley, K.A., 2020. U-loss associated with laser-heating of hematite and goethite in vacuum during (U–Th)/He dating and prevention using high O_2 partial pressure. Chem. Geol. 532, 119350. https://doi.org/10.1016/j.chemgeo.2019.119350.

Kalifi, A., Leloup, P.H., Sorrel, P., Galy, A., Demory, F., Spina, V., Huet, B., Quillévéré, F., Ricciardi, F., Michoux, D., 2021. Chronology of thrust propagation from an updated tectono-sedimentary framework of the Miocene molasse (western Alps). Solid Earth 12, 2735–2771.

Ketcham, R.A., Gautheron, C., Tassan-Got, L., 2011. Accounting for long alpha-particle stopping distances in (U–Th–Sm)/He geochronology: refinement of the baseline case. Geochim. Cosmochim. Acta 75, 7779–7791. https://doi.org/10.1016/j.gca.2011.10.011.

Kim, S.-T., O'Neil, J.R., 1997. Equilibrium and nonequilibrium oxygen isotope effects in synthetic carbonates. Geochim. Cosmochim. Acta 61, 3461–3475. https://doi.org/10.1016/S0016-7037(97)00169-5.

Krsnik, E., Methner, K., Campani, M., Botsyun, S., Mutz, S.G., Ehlers, T.A., Kempf, O., Fiebig, J., Schlunegger, F., Mulch, A., 2021. Miocene high elevation in the Central Alps. Solid Earth 12, 2615–2631. https://doi.org/10.5194/se-12-2615-2021.

Lacombe, O., Beaudoin, N.E., 2024. Timing, sequence, duration and rate of deformation in fold-and-thrust belts: a review of traditional approaches and recent advances from absolute dating (K–Ar illite/U–Pb calcite) of brittle structures. Comptes Rendus Géosci. 356, 1–28. https://doi.org/10.5802/crgeos.218.

Lardeaux, J.M., Schwartz, S., Tricart, P., Paul, A., Guillot, S., Béthoux, N., Masson, F., 2006. A crustal-scale cross-section of the south-western Alps combining geophysical and geological imagery. Terra Nova 18, 412–422. https://doi.org/10.1111/j.1365-3121.2006.00706.x.

Larroque, C., Delouis, B., Godel, B., Nocquet, J.M., 2009. Active deformation at the southwestern Alps-Ligurian basin junction (France–Italy boundary): evidence for recent change from compression to extension in the Argentera massif. Tectonophysics 467 (1–4), 22–34.

Lemot, F., Valla, P.G., van der Beek, P., Jagercikova, M., Niedermann, S., Carcaillet, J., Sobel, E.R., Andò, S., Garzanti, E., Robert, X., Balvay, M., Bernet, M., Glodny, J., Mocochain, L., 2023. Miocene cave sediments record topographic, erosional and drainage development in the Western European Alps. Earth Planet. Sci. Lett. 621, 118344. https://doi.org/10.1016/j.epsl.2023.118344.

Looser, N., Madritsch, H., Guillong, M., Laurent, O., Wohlwend, S., Bernasconi, S.M., 2021. Absolute age and temperature constraints on deformation along the basal décollement of the Jura fold-and-thrust belt from carbonate U-Pb dating and clumped isotopes. Tectonics 40,. https://doi.org/10.1029/2020TC006439. e2020TC006439.

Maino, M., Casini, L., Ceriani, A., Decarlis, A., Di Giulio, A., Seno, S., Setti, M., Stuart, F. M., 2015. Dating shallow thrusts with zircon (U-Th)/He thermochronometry—The shear heating connection. Geology 43, 495–498. https://doi.org/10.1130/G36492.1.

Malusà, M.G., Zhao, L., Eva, E., Solarino, S., Paul, A., Guillot, S., Schwartz, S., Dumont, T., Aubert, C., Salimbeni, S., Pondrelli, S., Wang, Q.C., Zhu, R.X., 2017. Earthquakes in the western Alpine mantle wedge. Gondwana Res. 44, 89–95.

Malusà, M.G., Guillot, S., Zhao, L., Paul, A., Solarino, S., Dumont, T., Schwartz, S., Aubert, C., Baccheschi, P., Eva, E., Lu, Y., Lyu, C., Pondrelli, S., Salimbeni, S., Sun, W., Yuan, H., 2021. The deep structure of the alps based on the CIFALPS seismic experiment: a synthesis. Geochem. Geophys. Geosystems 22(3), e2020GC009466. https://doi.org/10.1029/2020GC009466.

Manatschal, G., 2004. New models for evolution of magma-poor rifted margins based on a review of data and concepts from West Iberia and the Alps. Int. J. Earth Sci. 93, 432–466. https://doi.org/10.1007/s00531-004-0394-7.

Mangenot, X., Larmier, S., Girard, J.-P., Dyja-Person, V., Eiler, J.M., 2024. Diagenetic history of calcite fractures in Vaca Muerta shales (Argentina) inferred from paired Δ_{47} and fluid inclusion geothermometry. Mar. Pet. Geol. 160, 106630. https://doi.org/10.1016/j.marpetgeo.2023.106630.

Mathey, M., Walpersdorf, A., Sue, C., Baize, S., Deprez, A., 2020. Seismogenic potential of the High Durance Fault constrained by 20 yr of GNSS measurements in the Western European Alps. Geophys. J. Int. 222, 2136–2146. https://doi.org/10.1093/gji/ggaa292.

Mathey, M., Sue, C., Pagani, C., Baize, S., Walpersdorf, A., Bodin, T., Husson, L., Hannouz, E., Potin, B., 2021. Present-day geodynamics of the Western Alps: new insights from earthquake mechanisms. Solid Earth 12, 1661–1681. https://doi.org/10.5194/se-12-1661-2021.

Mathey, M., Doin, M.-P., André, P., Walpersdorf, A., Baize, S., Sue, C., 2022. Spatial heterogeneity of uplift pattern in the Western European alps revealed by InSAR time-series analysis. Geophys. Res. Lett. 49. e2021GL095744.

McDermott, R.G., Ault, A.K., Evans, J.P., Reiners, P.W., 2017. Thermochronometric and textural evidence for seismicity via asperity flash heating on exhumed hematite fault mirrors, Wasatch fault zone, UT, USA. Earth Planet. Sci. Lett. 471, 85–93. https://doi.org/10.1016/j.epsl.2017.04.020.

McDermott, R.G., Ault, A.K., Caine, J.S., 2021. Dating fault damage along the eastern Denali fault zone with hematite (U-Th)/He thermochronometry. Earth Planet. Sci. Lett. 563, 116872. https://doi.org/10.1016/j.epsl.2021.116872.

Mercier, D., 1977. Les modalités de la transgression jurassique dans la zone briançonnaise (Région de briançon, Hautes Alpes). Etude stratigraphique et sédimentologique (Theses). Université Pierre et Marie Curie - Paris VI.

Nouibat, A., Stehly, L., Paul, A., Schwartz, S., Bodin, T., Dumont, T., Rolland, Y., Brossier, R., Cifalps Team and AlpArray Working Group, 2022. Lithospheric transdimensional ambient-noise tomography of W-Europe: implications for crustal-scale geometry of the W-Alps. Geophys. J. Int. 229, 862–879. Doi: 10.1093/gji/ggab520.

Pagel, M., Bonifacie, M., Schneider, D.A., Gautheron, C., Brigaud, B., Calmels, D., Cros, A., Saint-Bezar, B., Landrein, P., Sutcliffe, C., Davis, D., Chaduteau, C., 2018. Improving paleohydrological and diagenetic reconstructions in calcite veins and breccia of a sedimentary basin by combining Δ_{47} temperature, $\delta^{18}O_{water}$ and U-Pb age. Chem. Geol. 481, 1–17. https://doi.org/10.1016/j.chemgeo.2017.12.026.

Parizot, O., Missenard, Y., Haurine, F., Blaise, T., Barbarand, J., Benedicto, A., Sarda, P., 2021. When did the Pyrenean shortening end? Insight from U-Pb geochronology of syn-faulting calcite (Corbières area, France). Terra Nova 33, 551–559. https://doi.org/10.1111/ter.12547.

Paton, C., Hellstrom, J., Paul, B., Woodhead, J., Hergt, J., 2011. Iolite: Freeware for the visualisation and processing of mass spectrometric data. J. Anal. at. Spectrom. 26, 2508. https://doi.org/10.1039/c1ja10172b.

Poage, M.A., Chamberlain, C.P., 2001. Empirical relationships between elevation and the stable isotope composition of precipitation and surface waters: considerations for studies of paleoelevation change. Am. J. Sci. 301, 1–15.

Poulain, P.A., 1977. Les eaux minérales et thermominérales dans le département des Hautes-Alpes- Alpes françaises. 197.

Reiners, P.W., Brandon, M.T., 2006. Using thermochronology to understand orogenic erosion. Annu. Rev. Earth Planet. Sci. 34, 419–466. https://doi.org/10.1146/annurev.earth.34.031405.125202.

Roberts, N., Holdsworth, R.E., 2022. Timescales of faulting through calcite geochronology: A review. J. Struct. Geol. 158, 104578.

Roberts, N.M.W., Rasbury, E.T., Parrish, R.R., Smith, C.J., Horstwood, M.S.A., Condon, D.J., 2017. A calcite reference material for LA-ICP-MS U-Pb geochronology. Geochem. Geophys. Geosystems 18, 2807–2814. https://doi.org/10.1002/2016GC006784.

Roberts, N.M.W., Walker, R.J., 2016. U-Pb geochronology of calcite-mineralized faults: absolute timing of rift-related fault events on the northeast Atlantic margin. Geology 44, 531–534. https://doi.org/10.1130/G37868.1.

Rolland, Y., Bilau, A., Cardinal, T., Nouibat, A., Bienveignant, D., Boschetti, L., Schwartz, S., Bernet, M., 2022. Bridging the gap between long-term orogenic evolution (>10 Ma Scale) and geomorphological processes that shape the western alps: insights from combined dating approaches. Geosciences 12, 393. https://doi.org/10.3390/geosciences12110393.

Royden, L., Burchfiel, B.C., 1989. Are systematic variations in thrust belt style related to plate boundary processes? (The western Alps versus the Carpathians). Tectonics 8, 51–61. https://doi.org/10.1029/TC008i001p00051.

Schmid, S., Kissling, E., 2000. The arc of the western Alps in the light of geophysical data on deep crustal structure. Tectonics 19, 62–85.

Schwartz, S., Lardeaux, J.M., Tricart, P., Guillot, S., Labrin, E., 2007. Diachronous exhumation of HP–LT metamorphic rocks from south-western Alps: evidence from fission-track analysis. Terra Nova 19, 133–140.

Schwartz, S., Tricart, P., Lardeaux, J.-M., Guillot, S., Vidal, O., 2009. Late tectonic and metamorphic evolution of the Piedmont accretionary wedge (Queyras Schistes lustrés, western Alps): evidences for tilting during Alpine collision. GSA Bull. 121, 502–518. https://doi.org/10.1130/B26223.1.

Schwartz, S., Gautheron, C., Audin, L., Dumont, T., Nomade, J., Barbarand, J., Pinna-Jamme, R., van der Beek, P., 2017. Foreland exhumation controlled by crustal thickening in the Western Alps. Geology 45, 139–142.

Schwartz, S., Rolland, Y., Nouibat, A., Boschetti, L., Bienveignant, D., Dumont, T., Mathey, M., Sue, C., Mouthereau, F., 2024. Role of mantle indentation in collisional deformation evidenced by deep geophysical imaging of Western Alps. Commun. Earth Environ. 5, 1–9. https://doi.org/10.1038/s43247-023-01180-y.

Selverstone, J., 2005. Are the alps collapsing? Annu. Rev. Earth Planet. Sci. 33, 113–132. https://doi.org/10.1146/annurev.earth.33.092203.122535.

Seward, D., Ford, M., Bürgisser, J., Lickorish, H., Williams, E.A., Meckel III, L.D., 1999. Preliminary results of fission-track analyses in the southern Pelvoux area. SE France. Mem. Sci. Geol. Padova 51, 25–31.

Simon-Labric, T., Rolland, Y., Dumont, T., Heymes, T., Authemayou, C., Corsini, M., Fornari, M., 2009. $^{40}Ar/^{39}Ar$ dating of Penninic Front tectonic displacement (W Alps) during the Lower Oligocene (31–34 Ma). Terra Nova 21, 127–136.

Smeraglia, L., Looser, N., Fabbri, O., Choulet, F., Guillong, M., Bernasconi, S.M., 2021. U-Pb dating of middle Eocene-Pliocene multiple tectonic pulses in the Alpine foreland. Solid Earth 12, 2539–2551. https://doi.org/10.5194/se-12-2539-2021.

Smeraglia, L., Fabbri, O., Choulet, F., Jaggi, M., Bernasconi, S.M., 2022. The role of thrust and strike-slip faults in controlling regional-scale paleofluid circulation in fold-and-thrust belts: Insights from the Jura Mountains (eastern France). Tectonophysics 829, 229299. https://doi.org/10.1016/j.tecto.2022.229299.

Sternai, P., Sue, C., Husson, L., Serpelloni, E., Becker, T.W., Willett, S.D., Faccenna, C., Di Giulio, A., Spada, G., Jolivet, L., Valla, P., Petit, C., Nocquet, J.-M., Walpersdorf, A., Castelltort, S., 2019. Present-day uplift of the European Alps: evaluating mechanisms and models of their relative contributions. Earth-Sci. Rev. 190, 589–604. https://doi.org/10.1016/j.earscirev.2019.01.005.

Sue, C., Delacou, B., Champagnac, J.-D., Allanic, C., Tricart, P., Burkhard, M., 2007. Extensional neotectonics around the bend of the Western/Central Alps: an overview. Int. J. Earth Sci. 96, 1101–1129. https://doi.org/10.1007/s00531-007-0181-3.

Sue, C., Tricart, P., 1999. Late alpine brittle extension above the Frontal Pennine Thrust near Briançon, western Alps. Eclogae Geol. Helvetiae 92, 171–181.

Sue, C., Tricart, P., 2003. Neogene to ongoing normal faulting in the inner western Alps: a major evolution of the late alpine tectonics. Tectonics 22(5), 1050..

Swart, P.K., Burns, S.J., Leder, J.J., 1991. Fractionation of the stable isotopes of oxygen and carbon in carbon dioxide during the reaction of calcite with phosphoric acid as a function of temperature and technique. Chem. Geol. Isot. Geosci. Sect. 86, 89–96. https://doi.org/10.1016/0168-9622(91)90055-2.

Tardy, M., Deville, E., Fudral, S., Guellec, S., Ménard, G., Thouvenot, F., Vialon, P., 1990. Interprétation structurale des données du profil de sismique réflexion profonde ECORS-CROP Alpes entre le front Pennique et la ligne du Canavese (Alpes occidentales). Mém. Socété Géologique Fr. 156, 217–226.

Thouvenot, F., Fréchet, J., 2006. Seismicity along the northwestern edge of the Adria microplate, in: The Adria Microplate: GPS Geodesy, Tectonics and Hazards. Springer, pp. 335–349.

Tricart, P., 1984. From passive margin to continental collision; a tectonic scenario for the Western Alps. Am. J. Sci. 284, 97–120.

Tricart, P., 2004. From extension to transpression during the final exhumation of the Pelvoux and Argentera massifs. Western Alps. Eclogae Geol. Helvetiae 97, 429–439. https://doi.org/10.1007/s00015-004-1138-1.

Tricart, P., Schwartz, S., Sue, C., Poupeau, G., Lardeaux, J.-M., 2001. La denudation tectonique de la zone ultradauphinoise et l'inversion du front brianconnais au sud-est du Pelvoux (Alpes occidentales); une dynamique miocene a actuelle. Bull. Société Géologique Fr. 172, 49–58.

Tricart, P., Lardeaux, J.-M., Schwartz, S., Sue, C., 2006. The late extension in the inner western Alps: a synthesis along the south-Pelvoux transect. Bull. Société Géologique Fr. 177, 299–310.

Tricart, P., Van Der Beek, P., Schwartz, S., Labrin, E., 2007. Diachronous late-stage exhumation across the western Alpine arc: constraints from apatite fission-track thermochronology between the Pelvoux and Dora-Maira Massifs. J. Geol. Soc. 164, 163–174. https://doi.org/10.1144/0016-76492005-174.

Vermeesch, P., 2018. IsoplotR: A free and open toolbox for geochronology. Geosci. Front. 9, 1479–1493. https://doi.org/10.1016/j.gsf.2018.04.001.

Vernant, P., Hivert, F., Chéry, J., Steer, P., Cattin, R., Rigo, A., 2013. Erosion-induced isostatic rebound triggers extension in low convergent mountain ranges. Geology 41, 467–470. https://doi.org/10.1130/G33942.1.

von Blanckenburg, F., Davies, J.H., 1995. Slab breakoff: a model for syncollisional magmatism and tectonics in the Alps. Tectonics 14, 120–131. https://doi.org/10.1029/94TC02051.

Walpersdorf, A., Pinget, L., Vernant, P., Sue, C., Deprez, A., the RENAG team, 2018. Does long-term GPS in the Western Alps finally confirm earthquake mechanisms? Tectonics 37, 3721–3737. https://doi.org/10.1029/2018TC005054.

Wernicke, R.S., Lippolt, H.J., 1994. 4He age discordance and release behavior of a double shell botryoidal hematite from the Schwarzwald. Germany. Geochim. Cosmochim. Acta 58, 421–429. https://doi.org/10.1016/0016-7037(94)90474-X.

Woodhead, J.D., Hergt, J.M., 2001. Strontium, Neodymium and Lead Isotope Analyses of NIST Glass Certified Reference Materials: SRM 610, 612, 614. Geostand. Geoanalytical Res. 25, 261–266. https://doi.org/10.1111/j.1751-908X.2001.tb00601.x.